Lewy pathology formation in patient-derived *GBA1* Parkinson's disease midbrain organoids

Emanuele Frattini,[1] Gaia Faustini,[2] Gianluca Lopez,[3] Emma V. Carsana,[4] Mattia Tosi,[1] Ilaria Trezzi,[1] Manuela Magni,[1] Giulia Soldà,[5,6] Letizia Straniero,[5,6] Daniele Facchi,[5,6] Maura Samarani,[7] Mitchell Martá-Ariza,[8,9] Chiara M. G. De Luca,[10] Elena Vezzoli,[11] Alessandra Pittaro,[3] Astghik Stepanyan,[12] Rosamaria Silipigni,[13] Isabel Rosety,[14] Jens C. Schwamborn,[14] Sergio P. Sardi,[15] Fabio Moda,[9] Stefania Corti,[1,16] Giacomo P. Comi,[1,16] Fabio Blandini,[17] Nicolas X. Tritsch,[18,19,†] Mario Bortolozzi,[20] Stefano Ferrero,[3,21] Fulvia M. Cribiù,[3,‡] Thomas Wisniewski,[8,22] Rosanna Asselta,[5,6] Massimo Aureli,[4] Arianna Bellucci[2] and Alessio Di Fonzo[1]

Abstract

Fibrillary aggregation of α-synuclein in Lewy body inclusions and nigrostriatal dopaminergic neuron degeneration define Parkinson's disease neuropathology. Mutations in *GBA1*, encoding glucocerebrosidase, are the most frequent genetic risk factor for Parkinson's disease. However, the lack of reliable experimental models able to reproduce key neuropathological signatures has hampered the clarification of the link between mutant glucocerebrosidase and Parkinson's disease pathology. Here, we describe an innovative protocol for the generation of human induced pluripotent stem cell-derived midbrain organoids containing dopaminergic neurons with nigral identity that reproduce characteristics of advanced maturation. When applied to patients with *GBA1*-related Parkinson's disease, this method enabled the differentiation of midbrain organoids recapitulating dopaminergic neuron loss and fundamental features of Lewy body pathology observed in human brains, including the generation of α-synuclein fibrillary aggregates with seeding activity that also propagate pathology in healthy control organoids. Still, we observed that the retention of mutant glucocerebrosidase in the endoplasmic reticulum and increased levels of

its substrate glucosylceramide are determinants of α-synuclein aggregation into Lewy body-like inclusions. Consistently, the reduction of glucocerebrosidase activity accelerated α-synuclein pathology by promoting fibrillary α-synuclein deposition. Finally, we demonstrated the efficacy of ambroxol and GZ667161 – two modulators of the glucocerebrosidase pathway in clinical development for the treatment of *GBA1*-related Parkinson's disease – in reducing α-synuclein pathology in this model, supporting the use of midbrain organoids as a relevant pre-clinical platform for investigational drug screening.

Author affiliations:

1 Neurology Unit, IRCCS Foundation Ca' Granda Ospedale Maggiore Policlinico, Milan 20122, Italy

2 Department of Molecular and Translational Medicine, University of Brescia, Brescia 25123, Italy

3 Division of Pathology, IRCCS Foundation Ca' Granda Ospedale Maggiore Policlinico, University of Milan, Milan 20122, Italy

4 Department of Medical Biotechnology and Translational Medicine, University of Milano, Milan 20054, Italy

5 Department of Biomedical Sciences, Humanitas University, Pieve Emanuele 20072, Italy

6 IRCCS Humanitas Research Hospital, Rozzano 20089, Italy

7 Unité de Trafic Membranaire et Pathogénèse, Département de Biologie Cellulaire et de l'Infection, Institut Pasteur, Paris 75015, France

8 Center for Cognitive Neurology, Department of Neurology, New York University Grossman School of Medicine, New York, NY 10016, USA

9 Institut de Neurociències, Universitat Autònoma de Barcelona, Barcelona, Spain

10 Division of Neurology 5 and Neuropathology, Fondazione IRCCS Istituto Neurologico Carlo Besta, Milan 20133, Italy

11 Advanced Light and Electron Microscopy BioImaging Centre (ALEMBIC), IRCCS San

Raffaele Scientific Institute, 20132 Milan, Italy

12 Chirurgia Generale 3, University Hospital of Padua, Padua 35128, Italy

13 IRCCS Foundation Ca' Granda Ospedale Maggiore Policlinico, Laboratorio di Genetica Medica, Milan 20122, Italy

14 Luxembourg Centre for Systems Biomedicine (LCSB), Developmental and Cellular Biology, University of Luxembourg, Belvaux L-4367, Luxembourg

15 Rare and Neurological Diseases Therapeutic Area, Sanofi, Framingham, MA 01701, USA

16 Department of Pathophysiology and Transplantation (DEPT), Dino Ferrari Centre, University of Milan, Milan 20122, Italy

17 Foundation IRCCS Ca' Granda Ospedale Maggiore Policlinico, Milan, Italy

18 Neuroscience Institute, New York University Grossman School of Medicine, New York, NY 10016, USA

19 Fresco Institute for Parkinson's and Movement Disorders, New York University Langone Health, New York, NY 10017, USA

20 Department of Physics and Astronomy "G. Galilei", Padua, Italy; Veneto Institute of Molecular Medicine (VIMM), Padua 35129, Italy

21 Department of Biomedical, Surgical, and Dental Sciences, University of Milan, Milan 20122, Italy

22 Department of Pathology and Department of Psychiatry, New York University Grossman School of Medicine, New York, NY 10016, USA

†Present address: Douglas Hospital Research Center, McGill University, Montreal, QC H4H 1R3, Canada

‡Present address: SC Anatomia e Istologia Patologica, Ospedale di Treviglio-Caravaggio-Ospedale di Romano di Lombardia ASST BG Ovest, Italy

Correspondence to: Alessio Di Fonzo, MD, PhD

Neurology Unit, IRCCS Foundation Ca' Granda Ospedale Maggiore Policlinico
Via Francesco Sforza 35, Milan 20122, Italy
E-mail: alessio.difonzo@policlinico.mi.it

Correspondence may also be addressed to: Emanuele Frattini, MD, PhD
Neurology Unit, IRCCS Foundation Ca' Granda Ospedale Maggiore Policlinico
Via Francesco Sforza 35, Milan 20122, Italy
E-mail: emanuele.frattini@policlinico.mi.it

Running title: Lewy-like pathology in midbrain organoids
Keywords: Parkinson's disease; midbrain organoids; Lewy bodies; *GBA1*; glucocerebrosidase; ambroxol

Introduction

Parkinson's disease (PD), caused predominantly by the degeneration of dopaminergic (DA) neurons in the midbrain substantia nigra (SN), is the most common neurodegenerative movement disorder[1] and an emerging public health concern in ageing population.[2] Lewy bodies (LBs) and Lewy neurites (LNs), insoluble inclusions affecting the cytoplasm and processes of neuronal cells, are defining neuropathological hallmarks of PD.[3] A heterogeneous mixture of proteins, membranes, and lipids accumulate in LB deposits, with α-synuclein (α-syn) fibrils being the major component.[4–6]

Mutations in the *GBA1* gene (*e.g.*, L444P), encoding the lysosomal glucosylceramide (GlcCer)-catalysing enzyme, glucocerebrosidase (GCase), are the most frequent genetic risk factor for PD.[7] GCase insufficiency due to biallelic *GBA1* mutations leads to cellular accumulation of GlcCer and causes Gaucher's disease (GD).[8] Interestingly, GD patients have a similar increased risk of developing PD to monoallelic *GBA1* mutation carriers.[9] Compelling evidence supports that mutant GCase misfolding and enzymatic deficiency, as well as accumulation of glycosphingolipid

substrates, drive α-syn aggregation in *GBA1*-related PD.[10–13] This notwithstanding, whether and how the impaired GCase pathway can induce α-syn pathological deposition and neuronal degeneration in PD remains to be determined. A main obstacle in this endeavour is the lack of reliable models able to faithfully recapitulate *GBA1*-PD neuropathology.

Here, we describe an innovative approach for the generation of human induced pluripotent stem cell (iPSC)-derived midbrain organoids (MOs) that contain mature DA neurons exhibiting key nigrostriatal-like characteristics and abundant neuromelanin pigmentation. This method was employed to investigate the link between mutant GCase and α-syn pathology in MOs from *GBA1*-PD patients. We found that *GBA1*-PD MOs present DA neurodegeneration and develop α-syn deposits recapitulating the major defining biochemical, immunohistochemical, ultrastructural, and morphological features of Lewy pathology observed in the brains of PD patients. Notably, these included efficient α-syn seeding activity as demonstrated by seed amplification assay (SAA) and by the propagation of α-syn fibrillary aggregates in healthy control MOs inoculated with *GBA1*-PD-derived insoluble protein extracts. Remarkably, we also found that the retention of mutant GCase in the endoplasmic reticulum (ER) and the increase of GlcCer resulting from impaired GCase activity are key drivers of α-syn pathology. Finally, we demonstrated that ambroxol and GZ667161, two modulators of the GCase pathway in clinical development for the treatment of *GBA1*-PD, reduce LB-like fibrillary α-syn deposition in patient-derived MOs, thus validating our model as a valuable pre-clinical tool for drug screening.

Materials and methods

Additional details can be found in the Supplementary material, Methods

Human samples

iPSC lines were generated from fibroblasts of a PD patient carrying the *GBA1* L444P heterozygous mutation (PD^{L444P}); a patient affected by both GD and PD carrying the *GBA1* L444P homozygous mutation (GD/PD^{L444P}); and two age- and gender-matched healthy donors with wild-type *GBA1* ($CTR1^{wt}$ and $CTR2^{wt}$). One additional control iPSC line ($CTR3^{wt}$) was purchased from the ATCC cell bank (#ACS-1023; American Type Culture Collection, Manassas, VA, USA).

Paraffin-embedded sections and fresh frozen tissue collected from the SN *pars compacta* of the

PD^{L444P} patient (SNc_PD^{L444P}), as well as of three healthy donors (SNc_CTR1^{wt}, SNc_CTR2^{wt}, and SNc_CTR3^{wt}) kindly supplied by the Parkinson's UK Brain Bank and used in Longhena et al.,[14] were used for immunostaining and biochemical analyses. Brain homogenates from three patients with PD (PD#1, PD#2, and PD#3) and two patients with multiple system atrophy type-P (MSA#1, MSA#2) were used for α-syn SAA.

The demographic data of donors of samples used in the study are illustrated in Supplementary Table 1 and discussed in Supplementary material – Clinical data.

Generation of MOs

iPSC lines were differentiated into MOs with a novel DA-patterning protocol adapted from Lancaster et al.[15] and Kriks et al.[16] On day 0, iPSCs were aggregated into embryoid bodies in 96-well ultra-low attachment plates and cultured in hES medium (DMEM/F12, 20% KSR, 3% FBS, 1% Glutamax, 1% MEM-NEAA) for 6 days. Embryoid bodies were subsequently transferred to 24-well ultra-low attachment plates and subdued to neural induction in a minimal medium (DMEM/F12, 1% N2 supplement, 1% Glutamax, 1% MEM-NEAA) for another 4 days. On day 11, tissues were embedded into Cultrex (R&D) and cultured in cerebral organoid medium (48% DMEM-F12, 48% Neurobasal, 0.5% N2 supplement, 0.4 µM Insulin, 1% Glutamax, 0.5% MEM-NEAA, 1% penicillin/streptomycin stock solution, 48 µM 2-Mercaptoethanol, and 1% B27 supplement without vitamin A) for 4 days. On day 14, organoids were transferred to spinning bioreactors (Corning) and cultured up to 150 days. In the spinner flask, MOs were cultured for 11 days in KSR medium (DMEM, 15% KSR, 1% MEM-NEAA, 1% penicillin/ampicillin stock solution, and 10 µM 2-Mercaptoethanol) and N2 medium (DMEM, 1% N2 supplement, and 1% penicillin/ampicillin stock solution) supplemented with 10 µM SB431542 (day 14-18), 100 nM LDN193189 (day 14-24), 2 µM purmorphamine (day 15-20), 250 nM SAG (day 15-20), 50 ng/ml FGF8b (day 15-20), 3 µM CHIR99021 (day 17-26). Following DA induction, MOs were maintained in B27 medium (Neurobasal, 2% B27 supplement, 1% Glutamax, and 1% penicillin/ampicillin stock solution) supplemented with BDNF 10 ng/ml, 10 ng/ml GDNF, 1 ng/ml TFGb3, 100 µM dibutyryl-cAMP, and 200 µM ascorbic acid.

Double 3D immunofluorescence staining of clarified whole MOs

MOs at 50, 100, and 150 DIV were fixed for 1 hour at room temperature in Immunofix and washed 3 times with PBS 0.1 M. Fixed MOs were permeabilized for 2 hours in PBS 0.1 M supplemented with 20% methanol and 0.1% Triton X-100, washed and incubated overnight at room temperature in blocking solution [10% normal goat serum (NGS), 0.1% Triton-X100 in PBS 0.1M] and then with primary antibodies at proper dilution (Supplementary Table 2) in blocking solution overnight for 5 days at room temperature. MOs were washed 3 times with 0.1% Triton-X100 PBS 0.1M for 24 hours and incubated with the fluorochrome-conjugated secondary antibodies (goat anti-mouse cy3 and goat anti-rabbit Alexa Fluor 488, Jackson Immunoresearch) in 0.1% Triton-X100 PBS 0.1 M plus 3 % NGS for 5 days at room temperature. After three washes in 0.1% Triton X-100 PBS for 24 hours, cells were clarified overnight in 47% 2,2'-thiodiethanol (TDE) and observed by means of a Zeiss confocal laser microscope LSM 880 with tile scan and z-stack reconstructions. Images (512 × 512 pixels) were then reconstructed using Zen lite 2.3.

Immunohistochemistry of PK-resistant α-syn in MOs and human brains

PK-resistant α-syn was visualized by chromogenic and fluorescent immunohistochemistry (IHC) using our previously described protocols.[17,18] Briefly, 8 µm thick sections from MOs and from the SN of the *GBA1*-PD donor patient of the PD^{L444P} iPSC line were deparaffinized and rehydrated through a series of xylene and ethanol washes. Sections were incubated with a working solution of PK (1:500; Enzo Life Sciences, catalog #ENZ-33801) for 20 minutes at 37°C. Further antigen retrieval was performed by treatment with 88% formic acid for 7 minutes, followed by boiling in citrate buffer (10 mM sodium citrate, 0.05% Tween-20; pH6). For chromogenic IHC only, endogenous peroxidase activity was blocked using 0.3% H_2O_2 for 20 minutes. Sections were blocked with 10% normal goat serum and incubated overnight at 4°C with either one of two anti-aggregated α-syn primary antibodies (BioLegend, cat# 847902, 1:100; BioLegend, cat# 824301, 1:200). For fluorescent IHC, sections were incubated with an anti-mouse IgG fluorescent or biotinylated secondary antibody (1:500, from Jackson ImmunoResearch, 2 hours at room temperature; or 1:1000, from Vector Labs, 1 hour at room temperature). For chromogenic IHC,

sections were incubated with ABC solution (1 hour at room temperature) followed by DAB. Later, sections were rinsed with water and counterstained with 0.25% Eosin Y for 15 seconds. Sections were dehydrated through a series of ethanol and xylene washes and coverslipped using ProLong™ Diamond Antifade Mountant (Invitrogen).

Results

iPSC-derived MOs display mature neuromelanin-containing DA neurons

MOs were generated from iPSCs of two PD patients with a L444P variant in *GBA1* (either monoallelic or biallelic, denominated PD^{L444P} and GD/PD^{L444P}, respectively) and of three healthy control donors with wild-type *GBA1* ($CTR1^{wt}$, $CTR2^{wt}$, $CTR3^{wt}$) (Supplementary Fig. 1 and Supplementary Table 1). Three independent clones of each line were differentiated into MOs with a novel protocol combining neuroectoderm induction[15] and ventral midbrain DA patterning[16] (Fig. 1A). iPSCs were aggregated into embryoid bodies (EBs) and cultured in low-dose bFGF/ high-dose ROCK inhibitor for 6 days. EBs that developed radial neuroepithelium were embedded into hydrogel droplets and transferred to spinning bioreactors for DA patterning and long-term maturation. MOs were cultured for up to 150 days *in vitro* (DIV) and collected at various time points of differentiation for extensive characterization and analyses.

Bulk RNA-sequencing profiling of differentiating MOs demonstrated progressive enrichment in neuronal and glial transcripts, as well as in key DA markers expressed during midbrain development (Supplementary Fig. 2A). Gene ontology enrichment analyses of differentially expressed genes across differentiation revealed upregulation of neuronal clusters and downregulation of cell proliferation markers (Supplementary Fig. 2B). The estimated fraction of neurons and astrocytes within MOs based on the expression of cell-specific marker genes[19] increased at later time points of analysis (Supplementary Fig. 2C). In differentiating MOs, the level of expression of well-established neuronal-specific and astrocyte-specific genes[20] progressively increased at later *in vitro* stages (Supplementary Fig. 2D and E). Specifically, expression levels of key DA genes of interest (*i.e.*, tyrosine hydroxylase – TH, dopamine receptor D2 – DRD2, and G-protein-regulated inward-rectifier potassium channel 2 – GIRK2) and of the astrocytic gene glial

fibrillary protein (GFAP) increased linearly over time (Supplementary Fig. 2F). Fluorescent *in situ* hybridization with RNAscope revealed signals for DRD2 and TH mRNA co-expression (Supplementary Fig. 2G). Genes associated with neurons of the SN and the ventral tegmental area (VTA)[21] were found to be expressed in mature MOs (Supplementary Fig. 2H), indicating that DA populations of diverse midbrain areas co-exist within mature MOs.

At fully differentiated time points, ~ 30% of $NeuN^+$ neurons stained positive for TH (Fig. 1B and C). Within MOs, we detected widespread and extended axonal projections expressing TH, which also co-colocalized with the post-mitotic neuronal marker MAP2 (Fig. 1D and E and Supplementary Video 1). TH^+ neurons expressed FOXA2 (Supplementary Fig. 3A) – indicating floor-plate derivation – as well as terminal-resident proteins DAT and VMAT2 (Supplementary Fig. 3B and C) – indicating synaptic maturation – and exhibited immunoreactivity for GIRK2 (Fig. 1F), which is peculiar to DA neurons. Non-DA neurons were detected by immunolabelling for GABAergic markers GAD65 and GAD67 (Supplementary Fig. 3D and E).

Along with neuronal cells, glial elements were progressively specified in MOs during differentiation. Astrocytes were detected by positive staining for GFAP and S100B and were abundantly represented, particularly at later time points (Supplementary Fig. 3F-I). Sparse oligodendroglial elements showed immunoreactivity for OLIG2 and the myelin-associated proteins MBP and CNPase (Supplementary Fig. 3H-J), demonstrating that MOs are a composite multicellular system with potential of reproducing neuron-glia interaction.

To investigate whether MOs recapitulate the typical membrane lipid composition of developmentally mature neurons, gangliosides were metabolically labelled at the steady state with the radioactive precursor [1-^{3}H]sphingosine. The glycosphingolipid (GSL) pattern was evaluated by high-performance thin-layer chromatography and radioactive lipids were visualized by digital autoradiography. Over the course of differentiation, the expression pattern of GSLs changed significantly, resembling the profile transition observed during neuronal development *in vivo*.[22] Specifically, early-stage MOs presented high content of GM3 and lower amounts of GM2, GM1 and GD1a components, whereas fully differentiated MOs at 65 DIV were enriched in all polysialogangliosides found in mature neurons of the adult brain, as well as in sphingomyelin, signifying their mature identity (Fig. 1G and Supplementary Fig. 3K and L).

As early as 35 DIV, we observed the appearance of pigmentation in the form of granular spots on

the surface of MOs (Fig. 1A and Supplementary Fig. 4A). High magnification brightfield microscopy imaging of hematoxylin-eosin-stained sections showed that the pigment was contained in cells with neuronal morphology (Fig. 1H and I and Supplementary Fig. 4B and C). Schmorl's ferricyanide reduction method for melanic pigments detected sites of reduction activity in MOs, which appeared as large, blue-stained granules within the neuronal cytosol, similar to deposits observed in human *post-mortem* SN sections (Fig. 1I and Supplementary Fig. 4D). Melanin sites corresponded to the same pigmented areas already visible in hematoxylin-eosin-stained slides, suggesting that the brown pigment contained within MOs was a type of melanin (Fig. 1I). To discriminate the pigment, we performed a red chromogen labelling of TH. The presence of pigmented granules in the cytoplasm of TH^+ neurons indicated the content of a type of melanin within DA neurons (Fig. 1J and Supplementary Fig. 4E). To better characterize the biosynthetic process of the pigment, we performed staining for tyrosinase (TYR), which catalyses the production of cutaneous melanin, but not of neuromelanin (NM).[23] First, we validated the antibody in a section of a nevus, which showed immunoreactivity for TYR and lack of expression of TH (Supplementary Fig. 4F). Pigmented neurons in MOs and in the SN section of a healthy donor subject displayed immunostaining of TH, but not of TYR (Supplementary Fig. 4F), suggesting that the melanin contained in MOs was in fact NM. Electron-dense, membrane-bound granules of 2-3 µm in size, some presenting a vacuolar lipid body, were detected in pigmented cells (Fig. Kand Supplementary Fig. 4G), thereby recapitulating the ultrastructural features of naturally occurring NM in human SN.[24] NM content progressively increased over time, covering up to ~ 80% of the total surface area of MOs at later stages of differentiation (Supplementary Fig. 4H).

Finally, the observation of Ca^{2+} transients in MOs indicated cellular activity, which was recorded in both basal conditions and upon incubation with either glutamic acid or dopamine (Supplementary Fig. 5A-G and Supplementary Video 2 and 3). In order to image Ca^{2+} events at a single-cell resolution, MOs were enzymatically dissociated into bidimensional cultures. Individual cells with typical neuronal morphology exhibited spontaneous Ca^{2+} surges of longer duration and lower firing rate, suggesting that a three-dimensional organization may contribute to activity complexity (Supplementary Video 4). Administration of tetrodotoxin suppressed Ca^{2+} events, indicating their dependency on Na^+ channel functional integrity (Supplementary Video 5).

Collectively, these results evidence that MOs contain mature DA neurons with post-natal nigral identity, resembling those found in human adult SN.

Mutant GCase is retained in the ER and leads to GlcCer increase in *GBA1*-PD MOs

GCase activity is reduced in brains and cerebrospinal fluid of PD patients with and without mutations in *GBA1* and is associated with increased levels of α-syn in brains of PD subjects.[25,26] However, whether GCase deficiency in PD leads to substrate accumulation and how GlcCer is implicated in the pathogenesis is still controversial.[27–30]

To establish a pharmacological model of GCase deficiency, CTR^{wt} MOs were treated with the GCase irreversible inhibitor Conduritol B Epoxide (CBE), which resulted in complete suppression of GCase activity (Fig. 2A). GD/PD^{L444P} MOs presented a marked reduction in the residual enzymatic activity (Fig. 2B). In PD^{L444P} MOs and in the SN of the PD^{L444P} donor patient (SNc_PD^{L444P}), GCase activity was reduced by ~ 50% with respect to wild-type *GBA1* (Fig. 2B and C). Similarly, the reduction in GCase protein amount observed in SNc_PD^{L444P} was reproduced in PD^{L444P} MOs (Fig. 2D-F and Supplementary Fig. 6A). GCase protein content was also reduced in GD/PD^{L444P} MOs and in CBE-treated CTR^{wt} MOs (Fig. 2D and E and Supplementary Fig. 6B and C).

To follow the intracellular fate of GCase, we treated cell lysates with endoglycosidase H (endo-H), which can discriminate glycoproteins retained in the ER from those that reached the mid-Golgi. In PD^{L444P} and GD/PD^{L444P} MOs (Supplementary Fig. 6D) and fibroblasts (not shown), most of GCase was endo-H-sensitive, in line with previous observations in mutant *GBA1* models.[11,31,32] By immunofluorescence analysis, we found that the ER protein Grp78, which can activate the unfolded protein response (UPR) upon interaction with misfolded proteins accumulated in the ER, was increased in PD^{L444P} and GD/PD^{L444P} MOs (Fig. 2G and H and Supplementary Fig. 6E). Since the levels of Grp78 are increased upon prolonged UPR activation, this would support the occurrence of ER stress.[33] Extensive co-localization of GCase with both Grp78 and the ER resident protein ERp72 in *GBA1* mutant MOs corroborated that most of the GCase protein was retained in the ER, likely in misfolded conformation (Fig. 2G and H and Supplementary Fig. 6E). Moreover, we detected increased levels of phospho-eIF2α in both PD^{L444P} and GD/PD^{L444P} MOs at 80 DIV, supporting activation of the UPR likely induced by ER-retained GCase (Fig. 2I and Supplementary

Fig. 6F). Interestingly, by Western blot analysis we found that the levels of Grp78 were higher in total protein extracts of PD^{L444P}, but not of GD/PD^{L444P} (Supplementary Fig. 6F and G), which may either indicate the occurrence of augmented ER stress in *GBA1*-related PD only or may reflect a higher cell loss in GD/PD^{L444P} MOs. Transmission electron microscopy (TEM) analysis showed a dilated morphology of ER lumen in *GBA1*-PD MOs, as seen in conditions of ER membrane expansion under ER stress[33] (Supplementary Fig. 6H). By contrast, in CTR^{wt} MOs only a fraction of GCase was located in the ER, but scarcely co-localized with Grp78 (Fig. 2G and H and Supplementary Fig. 6E).

We then explored whether the deficiency of GCase may lead to substrate accumulation. By metabolically labelling glycosphingolipids with [1-^{3}H]sphingosine, we observed accumulation of GlcCer in CBE-treated CTR^{wt} (Fig. 2J and Supplementary Fig. 6I). Of particular interest, *GBA1*-PD MOs also showed elevated levels of GlcCer, already observed at 65 DIV in GD/PD^{L444P} MOs and at 100 DIV in PD^{L444P} MOs (Fig. 2K and Supplementary Fig. 6J).

GBA1-PD MOs reproduce DA neurodegeneration and Lewy-like pathology

The degeneration of DA nigrostriatal neurons and the accumulation of insoluble α-syn in LBs and LNs are the defining neuropathological hallmarks of PD. *GBA1*-related PD brains also display neurodegeneration and Lewy pathology, as much as brains of GD patients with PD.[34,35]

We aimed to evaluate the capability of *GBA1* MOs to recapitulate DA neuron loss and to reproduce a clear α-syn pathology as seen in PD brains and its relation to mutant GCase. To this purpose, first we quantified the number of TH^+ cells vs the total number of $NeuN^+$ neurons in TDE-clarified whole MOs by three-dimensional confocal microscopy analysis and found a reduction in the amount of DA neurons in *GBA1* mutant MOs at 100 DIV, which was slightly more significant in GD/PD^{L444P} (Fig. 3A and B).

The analysis of total α-syn showed an incremental accumulation of the protein over time in TH^+ DA neurons of *GBA1*-PD MOs starting from 50 DIV (Fig. 3C and Supplementary Fig. 7A) and a higher content in PD^{L444P}, SNc_PD^{L444P} and after CBE treatment (Supplementary Fig. 7B-G). Notably, α-syn was detected in UREA/SDS reconstituted detergent-insoluble protein fraction from

GD/PD^{L444P} and PD^{L444P} MOs as early as 60 and 80 DIV, respectively (Fig. 3D and E). Similarly, CBE-treated CTR^{wt} MOs also exhibited detergent-insoluble α-syn (Supplementary Fig. 7H and I).

To further explore the aggregation state of detected insoluble α-syn, we performed both fluorescent and chromogenic IHC by first treating slides with proteinase K (PK) and then staining with two antibodies developed against fibrillary components of LBs (BioLegend, 847902; BioLegend, 824301). Remarkably, as of 80 DIV *GBA1* mutant MOs and CBE-treated samples displayed abundant insoluble Lewy-like deposits, resembling the neuropathology of the donor patient's brain (Fig. 3F and G and Supplementary Fig. 7J-L). Lewy-like aggregates displayed heterogeneous morphologies, ranging from diffuse cytoplasmic staining to discrete, packed structures and donut-shaped inclusions, reminiscent of mature LBs (Fig. 3H). Notably, both PD^{L444P} and GD/PD^{L444P} MOs also presented aggregated α-syn-immunoreactive neuronal processes, which were suggestive of Lewy-like neurites (Fig. 3I). In *GBA1*-mutated MOs, TH^{+} neurons also exhibited marked immunopositivity for α-syn phosphorylated at serine 129 (S129), a predominant post-translationally modified form of α-syn within LBs (Fig. 3J and K).[36,37] Additionally, double chromogenic immunostaining showed that α-syn inclusions in *GBA1*-PD MOs were also ubiquitinated (Supplementary Fig. 7M), like LBs in PD brains.[38]

To provide an ultrastructural characterization of aggregates and a validation of LB-like pathology, we performed TEM imaging, that revealed perinuclear inclusions of electron-dense material and membrane fragments within large autophagic vacuolar-like structures in *GBA1* MOs (Fig. 3L and Supplementary Fig. 8A). In some cells, the entire cytoplasm appeared to be crowded with membranous material originating from fragmented organelles (*e.g.*, mitochondria, lysosomes, autophagosomes), tubulovesicular structures, distorted vacuoles, lipids, randomly distributed filaments, and disrupted cytoskeleton (Fig. 3M and Supplementary Fig. 8B-D). Such features were fully reminiscent of the composition of *bona fide* LBs as detected by correlative light and electron microscopy and tomography in *post-mortem* PD brains.[5]

Taken together, these findings demonstrate that MOs from *GBA1* patients recapitulate fundamental morphological, immunohistochemical, and ultrastructural features of Lewy pathology.

α-syn produced in *GBA1* MOs seeds PD pathology

Evidence from PD brains and mouse models suggests that α-syn fibrils template the aggregation of endogenous α-syn and spread the pathology in interconnected neurons.[39] In our study, amyloid fibrils were found by TEM analysis of the insoluble α-syn fraction extracted from PD^{L444P} and GD/PD^{L444P} MOs (Supplementary Fig. 8E). Thioflavin-S (Thio-S) staining further demonstrated aggregates of fibrillary α-syn within TH^+ neurons in *GBA1* mutant and CBE-treated MOs (Fig. 4A-D and Supplementary Fig. 8F). To explore the seeding properties of the pathological form of α-syn found in the insoluble fraction, we performed SAA for ultrasensitive detection of aggregated α-syn. PD^{L444P} and GD/PD^{L444P} MOs, as well as SNc_PD^{L444P} and brain homogenates of subjects with α-synucleinopathy, induced an efficient seeding activity for recombinant α-syn (Fig. 4E and Supplementary Fig. 8G).

To corroborate the ability of α-syn fibrils from *GBA1*-PD MOs to self-propagate and induce aggregation in healthy cells, we injected PD^{L444P} MO-extracted α-syn insoluble fractions into CTR^{wt} MOs. Two weeks after the inoculation of fibrils from donor PD^{L444P} MOs, injected CTR^{wt} MOs developed Thio-S^+/α-syn^+ aggregates similar to those previously observed in the donor PD^{L444P} MOs (Fig. 4F and G).

These data indicate that α-syn produced in PD MOs shares similar seeding properties of that observed in PD brains.

α-syn/synapsin III interplay in *GBA1*-PD MOs

We then explored whether *GBA1* MOs may exhibit changes in the levels of synapsin III (Syn III), a pre-synaptic phosphoprotein co-accumulating and co-localizing with α-syn in LBs as it sticks to α-syn fibrils[14] and which acts as a key mediator of α-syn aggregation and toxicity.[40,41] In *GBA1*-PD MOs and in SNc_PD^{L444P}, we observed a significantly higher amount of Syn III, consistent with previous observations in PD brains (Supplementary Fig. 9A-D). Interestingly, Syn III levels increased earlier in biallelic *GBA1* MOs and later in the monoallelic *GBA1* mutants. Syn III also exhibited an increase, though not significant, after inhibition of GCase activity with CBE (Supplementary Fig. 9E and F). When we investigated the distribution of the protein in TH^+ neurons, we found that PD^{L444P} and GD/PD^{L444P} MOs exhibited a marked co-accumulation of Syn

III and α-syn, which were found to abundantly co-localize (Supplementary Fig. 9G and H), as observed in *post-mortem* PD brains.[14] Notably, levels of Syn III and α-syn showed a positive linear correlation in PD^{L444P} and GD/PD^{L444P} MOs (Supplementary Fig. 9I), corroborating the synergistic pathological interplay of these proteins in PD.[14]

GCase pathway modulation rescues α-syn pathology

Finally, we tested the capability of two compounds engaging with the GCase pathway to ultimately counteract neuronal loss and α-syn pathological deposition in *GBA1*-mutated MOs.

First, we treated MOs with ambroxol, a small molecule chaperone with proven efficacy in overcoming the retention of mutant GCase in the ER and in improving GCase activity.[32,42] Ambroxol administration led to an increase in the amount of GCase protein in MOs of all lines (Fig. 5A and B) and restored GCase enzymatic activity to normal levels in PD^{L444P} MOs, whereas it did not affect GCase activity in GD/PD^{L444P} MOs (Supplementary Fig. 10A). In PD^{L444P} and GD/PD^{L444P} MOs, the amount of GlcCer was not influenced by ambroxol treatment (Fig. 5E and Supplementary Fig. 10B). The higher co-localization between GCase and the lysosomal marker LAMP1 supported that ambroxol increased GCase targeting to the lysosome in both PD^{L444P} and GD/PD^{L444P} MOs (Fig. 5G and Supplementary Fig. 10C). In PD^{L444P} MOs, this was also accompanied by a reduction of the Grp78/GCase co-localization, suggesting a reduction of the misfolded fraction (Supplementary Fig. 10D-F). We then explored whether the observed effects of ambroxol on GCase activity and protein levels had an impact on DA neuron viability and α-syn pathology. Treatment with ambroxol rescued DA loss in PD^{L444P} MOs and improved, though not significantly, neuronal survival in GD/PD^{L444P} (Supplementary Fig. 11A and B). Ambroxol reduced the amount of total α-syn and Syn III in all samples (Supplementary Fig. 11C-F). Notably, the number and the area of PK-resistant α-syn aggregates were strongly reduced in *GBA1*-PD MOs (Fig. 5H and I and Supplementary Fig. 11G).

Secondly, we tested the effect of GZ667161, an experimental GlcCer synthase inhibitor which has been shown to decrease the levels of GlcCer and α-syn aggregates in *GBA1*$^{D409V+/+}$ and *SNCA*^{A53T} rodent models.[43] Upon treatment, GlcCer levels were undetectable (Fig. 5F and Supplementary Fig. 11H) and GCase protein amount was reduced in all samples (Fig. 5C and D). GZ6678161

improved the relocation of GCase to the lysosomal compartment, though this was significant only in GD/PD^{L444P} (Fig. 5G and Supplementary Fig. 10C), in which lysosomal accumulation of GlcCer is the main biochemical consequence of the enzymatic deficiency. These data may indicate that acting on lysosomal engorgement by reducing substrate accumulation could improve the upstream targeting of GCase from the ER to the lysosome. Importantly, GZ667161 reduced Grp78/GCase co-localization in PD^{L444P} MOs, suggesting also an effect on misfolding of GCase (Supplementary Fig. 10D-F). Cell counts of TH$^+$ cells showed that GZ667161 did not preserve DA neurons in PD^{L444P} and GD/PD^{L444P} (Supplementary Fig. 11A and B). Interestingly, levels of total α-syn were unaffected in *GBA1* MOs, though they were reduced in CTR^{wt} MOs (Supplementary Fig. 11I and J). However, GZ667161 treatment markedly reduced the load of PK-resistant α-syn aggregates and lowered Syn III levels (Fig. 5H and I and Supplementary Fig. 11G, K and L).

Discussion

The elucidation of pathogenic processes underlying neurodegeneration and development of novel therapies for PD both demand an experimental system that can recapitulate distinctive features of the human brain and fundamental hallmarks of neuropathology observed in patients. The bidimensional human cell models generated so far have failed to faithfully reproduce the characteristic features of DA neurons with mature SN-like identity and to replicate cardinal neuropathological signatures of PD. The advent of three-dimensional cultures of human DA neurons and midbrain-like organoids has reinvigorated this field.[44–49] Expanding this line of research, we devised a novel method for the generation of MOs which combines induction of neuroectoderm and DA patterning, ultimately allowing an advanced maturation state of neurons and glial cells. Unlike previously described methods for MO generation,[44–48] which apply DA patterning at the start of differentiation, the first part of our protocol consists of unpatterned neuroepithelium development and promotes the outgrowth and proliferation of neural progenitors, which are later subdued to small molecules guiding ventral midbrain development through activation of WNT signalling and SHH pathways. The timing of the start of the DA patterning at a later stage may favour a physiologically relevant environment in which a proportion of neural progenitors efficiently differentiate into DA neurons, while other precursors which have been partially committed to a non-DA fate (*e.g.*, other neuronal types, glia cells) continue their

differentiation path.

The progressively increasing expression of midbrain-specific transcripts and proteins in MOs supported their ability to reproduce key characteristics of adult human midbrain neurons, with both SN and VTA identity. The additional presence of cells expressing GABAergic and glial-specific markers further showed MOs to be a comprehensive multi-culture system mimicking the *in vivo* conditions.

The development of NM in MOs and its striking abundance at later stages of differentiation further evidenced the post-natal identity of our model. In human midbrain, NM contained in DA neurons confers the SN its characteristic pigmentation, becoming apparent after the third year of life and increasing in amount with age.[23] Although previous studies based on MO cultures claimed the presence of NM,[44,45,50–52] the lack of a full characterization of the observed pigment did not enable to clearly substantiate such evidence. Here, we determined whether the pigment developed by our MOs had the defining characteristics of naturally occurring NM of the human midbrain, according to stringent structural and immunohistochemical criteria.[23,24,53] The characterization of such pigment contained in electron-dense membrane-bound organelles exhibiting vacuolar lipid bulbs and progressively enriched in TH^+/TYR^- neurons demonstrated that our MO model develops NM granules in DA cells.

We then aimed at exploring the capability of MOs to model key *GBA1*-PD neuropathological features. To this end, we selected two subjects affected by PD and carrying the *GBA1* L444P mutation – the most common genetic risk factor for PD worldwide.[7] The implications of *GBA1* pathogenic variants in the pathogenesis of PD are still a matter of debate.[13] The known impact of GCase activity impairment in GD prompted studies investigating whether and how the enzymatic deficit could favour the aggregation of α-syn in neurons of *GBA1*-PD patients.[10,54] Interestingly, GlcCer accumulation has been reported in the SN of PD brains independently of *GBA1* mutational status.[27] However, in studies conducted on extra-nigral areas (*i.e.*, striatum, cerebellum, and cortex) of brains of PD subjects, substrate accumulation was not detected.[28–30] Whether this discrepancy is related to the fact that brain regions not primarily affected in PD may be less prone to show GlcCer accumulation or that substrate is not accumulated in PD still needs to be elucidated. Moreover, it is feasible that GlcCer accumulation may not be detectable in PD brains due to the loss of specific neuronal populations. In this regard, MOs can be evaluated before extensive

neuronal loss occurs, thus allowing to capture lipid dysregulation and toxic accumulation in the surviving DA neurons. Furthermore, by recapitulating features of the adult brain, the MO system allows a faithful reproduction of lipid metabolism occurring in neurons, thus letting to explore the repercussion of GlcCer metabolism on α-syn pathology. In line with the enzymatic/substrate hypothesis, *GBA1*-mutated MOs displayed a reduced GCase activity, a time-dependent increase in GlcCer levels, and substantial Lewy-like pathology. To the best of our knowledge, while there is no evidence of substrate accumulation comparable to that of Gaucher cells in models from *GBA1*-PD patients, we and two previous studies (conducted on iPSC-derived cultures of *GBA1* patients) detected higher levels of GlcCer.[12,55] Moreover, complete inhibition of GCase activity in control MOs treated with CBE also resulted in increased levels of GlcCer and α-synucleinopathy. This finding may be ascribed to the complete loss of enzymatic activity (which does not occur in mutant *GBA1* subjects), but also to other indirect off-target events, either impacting on GCase (one of which is the reduced protein amount) or α-syn metabolism.

On the other hand, the increased amount of GlcCer derived from GCase deficiency in *GBA1*-PD is unlikely the sole – or even primary – determinant of PD pathology. The similar risk of PD in carriers of one *GBA1* variant, who maintain a variably reduced GCase activity, and in GD patients, displaying a significant loss of enzymatic function, supports the hypothesis that factors other than GCase activity deficit play a role in *GBA1*-PD risk. Moreover, neuropathological studies in old GD subjects without PD did not detect α-syn pathology,[35] while specific *GBA1* variants with only a very mild impact on GCase activity (*e.g.*, E326K) are established risk factors of PD.[56] Exploring alternative scenarios to the enzymatic/substrate-centred hypothesis, it has been demonstrated that *GBA1* pathogenic mutations lead to the production of a misfolded GCase protein, which is retained in the ER and activates pathways associated with ER stress.[11,31,57] Mutant GCase undergoes ER-associated degradation, can interfere with chaperone-mediated autophagy and blocks lysosomal degradation of α-syn, thereby promoting α-syn aggregation.[11,31,58] Consistent with this hypothesis, we found that in *GBA1* MOs, mutant GCase was mainly located in the ER and extensively bound to the misfolded protein sensor Grp78, suggesting that most of the protein was retained in a misfolded state. The observation of ER membrane expansion and Grp78-mediated activation of UPR through phosphorylation of the pancreatic-like ER kinase (PERK) downstream effector eIF2α was supportive for ER stress response,[59,60] likely induced by ER accumulation of GCase. Interestingly, control MOs also displayed a low, but still detectable, amount of GCase co-localizing

with Grp78 in the absence of ER dilation. This finding either reproduces the physiological localization of properly folded GCase in the ER during the early stages of its maturation or suggests that a fraction of wild-type GCase requires the activation of Grp78 for efficient folding.

The relevance of these observations is strengthened when coupled to the extensive α-synucleinopathy observed in *GBA1*-PD MOs, as α-syn aggregation within LBs and LNs is a distinctive neuropathological finding in PD brains. Previous human iPSC-derived models did not convincingly recapitulate Lewy pathology. One study showed Thio-T-stained fibrils within TH^+ neurons in CRISPR-engineered isogenic MOs carrying the G2019S *LRRK2* mutation, but no evidence of α-syn fibrils was described.[50] Another study reported on LB-like inclusions in a genetically-modified model consisting of midbrain-like organoids derived from human embryonic stem cells in which *GBA1* was knocked out and α-syn was overexpressed.[61] A more recent work reported the presence of insoluble and S129 phosphorylated α-syn in *GBA1* mutant organoids.[47] Nevertheless, none of the previous studies exhaustively demonstrated that patient-derived MOs can develop α-syn deposits with the major features of authentic LBs, including decreased solubility, presence of fibrils, reactivity to amyloid-binding dyes, hyperphosphorylation at S129, seeding ability, and typical ultrastructural organization. Here, we reported that genetically unmodified MOs from subjects with *GBA1*-related PD developed insoluble α-syn aggregates in the shape of morphologically defined structures mirroring the typical LBs and LNs of PD neuropathology. The observed α-syn immunoreactive deposits ranged from punctate staining to variform compact inclusions, thereby representing diverse stages of the formation process of Lewy aggregates.[62] Moreover, in addition to the presence of insoluble α-syn and of S129 phosphorylated and ubiquitinated α-syn, the localization of Thio-S/α-syn double-positive inclusions in TH^+ neurons in *GBA1*-PD MOs reflected the classical fibrillary organization of α-syn in DA neurons of PD brains. The demonstration that LB-like inclusions in *GBA1* mutant MOs are enriched in crowded organelles and membrane fragments, tubulovesicular structures, and aberrantly distributed filaments validates the ability of this model to also closely mimic aspects of the ultrastructural composition of *bona fide* LB pathology. Strikingly, the similar seeding activity for α-syn displayed by *GBA1*-PD MOs and brain homogenates in SAA and upon the injection in healthy MOs supported that the α-syn aggregates/polymorphs from MOs and *post-mortem* PD brains share similar properties, indicating that this experimental model can appropriately recapitulate key aspects of patients' pathology.

It is noteworthy that, while we reported marked aggregation of α-syn in heterozygous as well as in homozygous *GBA1* MOs, we observed an increase in total α-syn content only in the heterozygous PD and not in the GD/PD. One possible explanation could be that the almost complete loss of GCase activity in GD may result in a more pronounced oxidative stress, that in turn would enhance α-syn misfolding and aggregation.[63] Consistently, it has been found that α-syn has an increased tendency to form dimers in the erythrocyte membrane of GD patients, and this is related to both the level of lipids, like GlcCer, and the increased oxidative stress observed in the context of GCase deficiency.[64] Still, the observation that in homozygous *GBA1* MOs total α-syn accumulates selectively in TH^+ neurons supports the relevance of this model to recapitulate fundamental pathological events in PD and warrants further studies to investigate the multiplicity of mechanisms behind α-syn pathology.

An additional question which our study tried to address pertains the temporal relationship between GCase defects and α-synucleinopathy. In the heterozygous and homozygous *GBA1* mutant MOs, the initial accumulation of α-syn within TH^+ neurons, which is seemingly the first step of the aggregation process, occurred at the same stage (*i.e.*, 50 DIV). However, the fact that the GlcCer amount was normal in the heterozygous at 65 DIV suggested that substrate content, which reflects the residual GCase activity, did not play an initiating role in α-syn pathology. Similarly, the observation of Lewy-like inclusions at an earlier time point than GlcCer increase in the monoallelic *GBA1* PD^{L444P} MOs supports this hypothesis. This having been established, the earlier conversion of α-syn into insoluble forms in GD/PD^{L444P} (*i.e.*, 60 DIV) compared with PD^{L444P} (*i.e.*, 80 DIV) suggested a more rapid progression of PD pathology. This could be explained by the earlier increase in the amount of GlcCer, which may act as a modulating factor in the dynamics of α-syn pathology, in line with recent observations in models of GCase inhibition.[54] Interestingly, the levels of Syn III, a pre-synaptic phosphoprotein found in LBs and implicated in α-syn aggregation,[14,40,41] also increased earlier in GD/PD^{L444P} MOs, supporting an accelerated aggregation process.

Finally, we investigated the potential of MOs as a patient-derived model for the screening of candidate therapeutic compounds. While enzyme replacement therapy and substrate reduction therapy are approved treatments to address GCase insufficiency in GD, there is no specific therapy for *GBA1*-related PD. Tackling impaired GCase metabolism to act on downstream effects of α-syn accumulation is a rapidly expanding avenue of research in drug development for PD. Molecules engaging with the GCase pathway have entered clinical trials for PD, including the open-label

clinical trial testing ambroxol[65] (NCT02941822) and the phase II trial on the GlcCer synthase inhibitor venglustat[66] (NCT02906020). The observations of mutated GCase undergoing aberrant post-translational folding increasingly clarify the mechanism by which ER-retained GCase induces unfolded protein response and α-syn aggregation.[11] In this respect, ambroxol may modulate α-syn pathology by assisting the correct folding of GCase in the ER and facilitating its trafficking to the lysosome.[32] In our study, ambroxol proved to increase the levels of GCase protein in MOs of both *GBA1*-mutated patients, to improve the trafficking of the enzyme to its physiological lysosomal location, and to significantly reduce the load of Lewy-like pathology. Notably, the observation that ambroxol-treated GD/PD^{L444P} MOs did not increase GCase activity and that GlcCer levels were not affected in *GBA1* mutants suggested that the rescue of α-syn aggregates was not directly linked to the enzyme function. Moreover, even when GCase activity was restored as observed in the heterozygous *GBA1* MO, GlcCer levels remained higher than in wild-type MOs, suggesting either that ambroxol directs GCase partly to non-lysosomal compartments or that GlcCer also accumulates in membrane domains other than the lysosome.[67]

Exploring the hypothesis of GlcCer accumulation as a major player in α-syn pathology, we also tested the GlcCer synthase inhibitor GZ667161, which completely suppressed new production of GlcCer in MOs. Notably, treatment with GZ667161 markedly attenuated Lewy-like pathology, in line with previous observations in GD and PD mouse models.[43] Levels of total α-syn, unlike the aggregated form, were not affected by exposure to GZ667161. This observation suggested that GlcCer favours the conversion of physiological α-syn to its insoluble form, while the reduction of GlcCer amount shifts the soluble/insoluble α-syn balance towards its physiological, soluble form. Therefore, GZ667161 appears to efficiently overcome one of the main limitations associated with α-syn clearing strategies, that is the development of a possible soluble "α-synucleinopenia".[68] Interestingly, Syn III, which co-aggregates with α-syn in LB fibrils, was also reduced by the treatment. One possible explanation may imply a GlcCer-dependent remodelling of membranes, which could prevent the formation of new aggregates and, by favouring soluble α-syn increase, allow a more efficient dispersion of synaptic vesicles, with which Syn III interacts.[69] The reciprocal regulation of α-syn and Syn III in synaptic vesicle release is sustained by findings showing that Syn III is low in wild-type mice with physiological levels of soluble α-syn, while α-syn null mice, as well as animals that by developing pathological α-syn aggregates display a loss of function of soluble α-syn, exhibit increased Syn III accumulation and synaptic vesicle clumping.[40,41,69]

Alternatively, by favouring the degradation of Syn III, which acts as α-syn fibril stabilizer, GZ667161 leads to fibrils reduction, thus reproducing the same α-syn pathology rescue observed following *in vivo* Syn III gene silencing in transgenic mice.[70] However, the precise mechanism by which GlcCer synthase inhibition results in the attenuation of α-syn pathology demands further investigation. Likewise, we need to deepen the significance of GCase retention within the ER and its impact on α-syn pathology.

Lastly, the potential of ambroxol and GZ667161 to have an impact on the survival of neurons in PD remains an essential point to be clarified. While our results support the use of ambroxol in the heterozygous *GBA1* PD for improved neuronal survival, our experiments with ambroxol in GD/PD and with GZ667161 did not meet this endpoint and agree with recent results on the effect of venglustat in *GBA1*-mutated mice overexpressing human α-syn.[71] Our data support that, although ambroxol and GZ667161 are both able to significantly reduce α-syn pathology, the different effect exerted by these compounds on GCase levels and activity, either increased by ambroxol or not as in the case of GZ667161, may underlie their diverse impact on neuronal survival. It should also be pointed out that in our study drug testing was carried out when neurodegeneration had already been established (*i.e.*, at DIV 100) and it could be speculated that an earlier timing for pharmacological intervention may instead have exerted a neuroprotective effect.

In conclusion, we present an innovative MO-based culture system derived from patients with *GBA1*-PD capable of reproducing key features of Lewy pathology and neurodegeneration. The concomitant occurrence of α-synucleinopathy in mono- and biallelic *GBA1* MOs suggests a shared common initiating event for both, likely misfolded mutant GCase retained in the ER. Still, the severity of GCase activity reduction and Syn III increase may act as accelerating factors in the progression of α-syn pathology by favouring the conversion of soluble α-syn to its insoluble forms. Finally, the observation of α-syn pathology rescue with ambroxol and GZ667161, that act at different levels of the GCase pathway, endorses the employment of MOs as a patient-specific tool for a broader implementation of personalized medicine.

Data availability

RNA-seq data are deposited in the Zenodo repository

(https://doi.org/10.5281/zenodo.5607334) with restricted access and are available on request. The data are not publicly available because they contain information that could compromise research participant consent and privacy. Requests to access the data should be sent to biblioteca@humanitas.it.

Acknowledgements

We thank M. Brevi, G. Alfonsi, E. Bistaffa, M. Pannella, G. Pires and the NYU Center for Biospecimen Research and Development for processing of specimen; F. Carubbi and F. Nascimbeni of the University of Modena and Reggio Emilia for providing clinical and biological material. We also acknowledge ALEMBIC (Advanced Light and Electron Microscopy BioImaging Center) at IRCCS Ospedale San Raffaele for EM analyses; Euro-BioImaging (www.eurobioimaging.eu) for providing access to imaging technologies and services via the Italian Node (ALEMBIC, Milan, Italy). The authors warmly remember co-investigators Professor Stefano Duga (16/09/1967-10/11/2021), geneticist, and Professor Nereo Bresolin (25/08/1952 – 02/05/2023), neurologist, for their enthusiasm and inspiration over the years.

Funding

PRIN 2017228L3J (RA, MA, and MB); Italian Ministry of Health RRC (ADF); Fondazione Cariplo 2015–1017 (MA); Italian Ministry of Health RRC (FM); Italian Ministry of Health GR-2021-12372019 (FM); Italian Ministry of Health PNRR-MAD-2022-12376035 (FM); NIH/NIA P30AG066512 (TW); NIH/NIA P01AG060882 (TW); Fondazione Grigioni per il Morbo di Parkinson (LS); Fresco Institute for Parkinson's and Movement Disorders (EF, NXT, and ADF). The authors would like to acknowledge the Dino Ferrari Center and Mizutani Foundation for Glycoscience for support.

Competing interests

Authors declare that they have no competing interests. S.P.S. is an employee and stockholder of

Sanofi. He provided the molecule GZ667161 that was tested in midbrain organoids. To avoid potential biases, this author was excluded from experiments and analysis of data concerning use of GZ667161 in midbrain organoids. No research funding was obtained from any company for the present study.

Supplementary material

Supplementary material is available at *Brain* online.

References

1. Feigin VL, Nichols E, Alam T, et al. Global, regional, and national burden of neurological disorders, 1990–2016: a systematic analysis for the Global Burden of Disease Study 2016. *Lancet Neurol*. 2019;18(5):459-480. doi:10.1016/S1474-4422(18)30499-X

2. United Nations Department of Economic and Social Affairs, Population Division. *World Population Ageing 2015*.

3. Goedert M, Spillantini MG, Del Tredici K, Braak H. 100 years of Lewy pathology. *Nat Rev Neurol*. 2013;9(1):13-24. doi:10.1038/nrneurol.2012.242

4. Spillantini MG, Schmidt ML, Lee VM, Trojanowski JQ, Jakes R, Goedert M. Alpha-synuclein in Lewy bodies. *Nature*. 1997;388(6645):839-840. doi:10.1038/42166

5. Shahmoradian SH, Lewis AJ, Genoud C, et al. Lewy pathology in Parkinson's disease consists of crowded organelles and lipid membranes. *Nat Neurosci*. 2019;22(7):1099-1109. doi:10.1038/s41593-019-0423-2

6. Fares MB, Jagannath S, Lashuel HA. Reverse engineering Lewy bodies: how far have we come and how far can we go? *Nat Rev Neurosci*. 2021;22(2):111-131. doi:10.1038/s41583-020-00416-6

7. Sidransky E, Nalls MA, Aasly JO, et al. Multicenter analysis of glucocerebrosidase mutations in Parkinson's disease. *N Engl J Med*. 2009;361(17):1651-1661. doi:10.1056/NEJMoa0901281

8. Grabowski GA. Phenotype, diagnosis, and treatment of Gaucher's disease. *Lancet Lond Engl*. 2008;372(9645):1263-1271. doi:10.1016/S0140-6736(08)61522-6

9. Riboldi GM, Di Fonzo AB. GBA, Gaucher Disease, and Parkinson's Disease: From Genetic to Clinic to New Therapeutic Approaches. *Cells*. 2019;8(4):364. doi:10.3390/cells8040364

10. Mazzulli JR, Xu YH, Sun Y, et al. Gaucher disease glucocerebrosidase and α-synuclein form a bidirectional pathogenic loop in synucleinopathies. *Cell*. 2011;146(1):37-52. doi:10.1016/j.cell.2011.06.001

11. Maor G, Rencus-Lazar S, Filocamo M, Steller H, Segal D, Horowitz M. Unfolded protein response in Gaucher disease: from human to Drosophila. *Orphanet J Rare Dis*. 2013;8(1):140. doi:10.1186/1750-1172-8-140

12. Schöndorf DC, Aureli M, McAllister FE, et al. iPSC-derived neurons from GBA1-associated Parkinson's disease patients show autophagic defects and impaired calcium homeostasis. *Nat Commun*. 2014;5:4028. doi:10.1038/ncomms5028

13. Smith L, Schapira AHV. GBA Variants and Parkinson Disease: Mechanisms and Treatments. *Cells*. 2022;11(8):1261. doi:10.3390/cells11081261

14. Longhena F, Faustini G, Varanita T, et al. Synapsin III is a key component of α-synuclein fibrils in Lewy bodies of PD brains. *Brain Pathol Zurich Switz*. 2018;28(6):875-888. doi:10.1111/bpa.12587

15. Lancaster MA, Knoblich JA. Generation of cerebral organoids from human pluripotent stem cells. *Nat Protoc*. 2014;9(10):2329-2340. doi:10.1038/nprot.2014.158

16. Kriks S, Shim JW, Piao J, et al. Dopamine neurons derived from human ES cells efficiently engraft in animal models of Parkinson's disease. *Nature*. 2011;480(7378):547-551. doi:10.1038/nature10648

17. Drummond E, Nayak S, Ueberheide B, Wisniewski T. Localized Proteomics of Individual Neurons Isolated from Formalin-Fixed, Paraffin-Embedded Tissue Sections Using Laser Capture Microdissection. In: Santamaría E, Fernández-Irigoyen J, eds. *Current Proteomic Approaches Applied to Brain Function*. Vol 127. Neuromethods. Springer New York; 2017:289-301. doi:10.1007/978-1-4939-7119-0_18

18. Drummond E, Nayak S, Pires G, Ueberheide B, Wisniewski T. Isolation of Amyloid Plaques and Neurofibrillary Tangles from Archived Alzheimer's Disease Tissue Using Laser-Capture Microdissection for Downstream Proteomics. *Methods Mol Biol Clifton NJ*. 2018;1723:319-334. doi:10.1007/978-1-4939-7558-7_18

19. McKenzie AT, Wang M, Hauberg ME, et al. Brain Cell Type Specific Gene Expression and Co-expression Network Architectures. *Sci Rep*. 2018;8(1):8868. doi:10.1038/s41598-018-27293-5

20. Sloan SA, Darmanis S, Huber N, et al. Human Astrocyte Maturation Captured in 3D Cerebral Cortical Spheroids Derived from Pluripotent Stem Cells. *Neuron*. 2017;95(4):779-790.e6. doi:10.1016/j.neuron.2017.07.035

21. Poulin JF, Zou J, Drouin-Ouellet J, Kim KYA, Cicchetti F, Awatramani RB. Defining midbrain dopaminergic neuron diversity by single-cell gene expression profiling. *Cell Rep*. 2014;9(3):930-943. doi:10.1016/j.celrep.2014.10.008

22. Svennerholm L, Boström K, Fredman P, Månsson JE, Rosengren B, Rynmark BM. Human brain gangliosides: developmental changes from early fetal stage to advanced age. *Biochim Biophys Acta*. 1989;1005(2):109-117. doi:10.1016/0005-2760(89)90175-6

23. Zecca L, Bellei C, Costi P, et al. New melanic pigments in the human brain that accumulate in aging and block environmental toxic metals. *Proc Natl Acad Sci U S A*. 2008;105(45):17567-17572. doi:10.1073/pnas.0808768105

24. Moses HL, Ganote CE, Beaver DL, Schuffman SS. Light and electron microscopic studies of pigment in human and rhesus monkey substantia nigra and locus coeruleus. *Anat Rec*. 1966;155(2):167-183. doi:10.1002/ar.1091550205

25. Gegg ME, Burke D, Heales SJR, et al. Glucocerebrosidase deficiency in substantia nigra of parkinson disease brains. *Ann Neurol*. 2012;72(3):455-463. doi:10.1002/ana.23614

26. Parnetti L, Chiasserini D, Persichetti E, et al. Cerebrospinal fluid lysosomal enzymes and alpha-synuclein in Parkinson's disease. *Mov Disord Off J Mov Disord Soc*. 2014;29(8):1019-1027. doi:10.1002/mds.25772

27. Huebecker M, Moloney EB, van der Spoel AC, et al. Reduced sphingolipid hydrolase activities, substrate accumulation and ganglioside decline in Parkinson's disease. *Mol Neurodegener*. 2019;14(1):40. doi:10.1186/s13024-019-0339-z

28. Gegg ME, Sweet L, Wang BH, Shihabuddin LS, Sardi SP, Schapira AHV. No evidence for substrate accumulation in Parkinson brains with GBA mutations. *Mov Disord Off J Mov Disord Soc*. 2015;30(8):1085-1089. doi:10.1002/mds.26278

29. Boutin M, Sun Y, Shacka JJ, Auray-Blais C. Tandem Mass Spectrometry Multiplex Analysis of Glucosylceramide and Galactosylceramide Isoforms in Brain Tissues at Different Stages of Parkinson Disease. *Anal Chem*. 2016;88(3):1856-1863. doi:10.1021/acs.analchem.5b04227

30. Leyns CEG, Prigent A, Beezhold B, et al. Glucocerebrosidase activity and lipid levels are related to protein pathologies in Parkinson's disease. *Npj Park Dis*. 2023;9(1):74. doi:10.1038/s41531-023-00517-w

31. Ron I, Horowitz M. ER retention and degradation as the molecular basis underlying Gaucher disease heterogeneity. *Hum Mol Genet*. 2005;14(16):2387-2398. doi:10.1093/hmg/ddi240

32. Bendikov-Bar I, Ron I, Filocamo M, Horowitz M. Characterization of the ERAD process of the L444P mutant glucocerebrosidase variant. *Blood Cells Mol Dis*. 2011;46(1):4-10. doi:10.1016/j.bcmd.2010.10.012

33. Hetz C. The unfolded protein response: controlling cell fate decisions under ER stress and beyond. *Nat Rev Mol Cell Biol*. 2012;13(2):89-102. doi:10.1038/nrm3270

34. Tayebi N, Walker J, Stubblefield B, et al. Gaucher disease with parkinsonian manifestations: does glucocerebrosidase deficiency contribute to a vulnerability to parkinsonism? *Mol Genet Metab*. 2003;79(2):104-109. doi:10.1016/s1096-7192(03)00071-4

35. Wong K, Sidransky E, Verma A, et al. Neuropathology provides clues to the pathophysiology of Gaucher disease. *Mol Genet Metab*. 2004;82(3):192-207. doi:10.1016/j.ymgme.2004.04.011

36. Fujiwara H, Hasegawa M, Dohmae N, et al. α-Synuclein is phosphorylated in synucleinopathy lesions. *Nat Cell Biol*. 2002;4(2):160-164. doi:10.1038/ncb748

37. Anderson JP, Walker DE, Goldstein JM, et al. Phosphorylation of Ser-129 is the dominant pathological modification of alpha-synuclein in familial and sporadic Lewy body disease. *J Biol Chem*. 2006;281(40):29739-29752. doi:10.1074/jbc.M600933200

38. Kuzuhara S, Mori H, Izumiyama N, Yoshimura M, Ihara Y. Lewy bodies are ubiquitinated. A light and electron microscopic immunocytochemical study. *Acta Neuropathol (Berl)*. 1988;75(4):345-353. doi:10.1007/BF00687787

39. Henderson MX, Cornblath EJ, Darwich A, et al. Spread of α-synuclein pathology through the brain connectome is modulated by selective vulnerability and predicted by network analysis. *Nat Neurosci*. 2019;22(8):1248-1257. doi:10.1038/s41593-019-0457-5

40. Faustini G, Longhena F, Varanita T, et al. Synapsin III deficiency hampers α-synuclein aggregation, striatal synaptic damage and nigral cell loss in an AAV-based mouse model of Parkinson's disease. *Acta Neuropathol (Berl)*. 2018;136(4):621-639. doi:10.1007/s00401-018-1892-1

41. Faustini G, Longhena F, Bruno A, et al. Alpha-synuclein/synapsin III pathological interplay boosts the motor response to methylphenidate. *Neurobiol Dis*. 2020;138:104789. doi:10.1016/j.nbd.2020.104789

42. Magalhaes J, Gegg ME, Migdalska-Richards A, Schapira AH. Effects of ambroxol on the autophagy-lysosome pathway and mitochondria in primary cortical neurons. *Sci Rep*. 2018;8(1):1385. doi:10.1038/s41598-018-19479-8

43. Sardi SP, Viel C, Clarke J, et al. Glucosylceramide synthase inhibition alleviates aberrations in synucleinopathy models. *Proc Natl Acad Sci U S A*. 2017;114(10):2699-2704. doi:10.1073/pnas.1616152114

44. Jo J, Xiao Y, Sun AX, et al. Midbrain-like Organoids from Human Pluripotent Stem Cells Contain Functional Dopaminergic and Neuromelanin-Producing Neurons. *Cell Stem Cell*. 2016;19(2):248-257. doi:10.1016/j.stem.2016.07.005

45. Monzel AS, Smits LM, Hemmer K, et al. Derivation of Human Midbrain-Specific Organoids from Neuroepithelial Stem Cells. *Stem Cell Rep*. 2017;8(5):1144-1154. doi:10.1016/j.stemcr.2017.03.010

46. Fiorenzano A, Sozzi E, Birtele M, et al. Single-cell transcriptomics captures features of human midbrain development and dopamine neuron diversity in brain organoids. *Nat Commun*. 2021;12(1):7302. doi:10.1038/s41467-021-27464-5

47. Baden P, Perez MJ, Raji H, et al. Glucocerebrosidase is imported into mitochondria and preserves complex I integrity and energy metabolism. *Nat Commun*. 2023;14(1):1930. doi:10.1038/s41467-023-37454-4

48. Reumann D, Krauditsch C, Novatchkova M, et al. In vitro modeling of the human dopaminergic system using spatially arranged ventral midbrain–striatum–cortex assembloids. *Nat Methods*. 2023;20(12):2034-2047. doi:10.1038/s41592-023-02080-x

49. Galet B, Cheval H, Ravassard P. Patient-Derived Midbrain Organoids to Explore the Molecular Basis of Parkinson's Disease. *Front Neurol*. 2020;11:1005. doi:10.3389/fneur.2020.01005

50. Kim H, Park HJ, Choi H, et al. Modeling G2019S-LRRK2 Sporadic Parkinson's Disease in 3D Midbrain Organoids. *Stem Cell Rep*. 2019;12(3):518-531. doi:10.1016/j.stemcr.2019.01.020

51. Kwak TH, Kang JH, Hali S, et al. Generation of homogeneous midbrain organoids with in vivo-like cellular composition facilitates neurotoxin-based Parkinson's disease modeling. *Stem Cells Dayt Ohio*. 2020;38(6):727-740. doi:10.1002/stem.3163

52. Smits LM, Reinhardt L, Reinhardt P, et al. Modeling Parkinson's disease in midbrain-like organoids. *NPJ Park Dis*. 2019;5:5. doi:10.1038/s41531-019-0078-4

53. Tribl F, Arzberger T, Riederer P, Gerlach M. Tyrosinase is not detected in human catecholaminergic neurons by immunohistochemistry and Western blot analysis. In: Gerlach M, Deckert J, Double K, Koutsilieri E, eds. *Neuropsychiatric Disorders An Integrative Approach*. Vol 72. Journal of Neural Transmission. Supplementa. Springer Vienna; 2007:51-55. doi:10.1007/978-3-211-73574-9_8

54. Henderson MX, Sedor S, McGeary I, et al. Glucocerebrosidase Activity Modulates Neuronal Susceptibility to Pathological α-Synuclein Insult. *Neuron*. 2020;105(5):822-836.e7. doi:10.1016/j.neuron.2019.12.004

55. Burbulla LF, Jeon S, Zheng J, Song P, Silverman RB, Krainc D. A modulator of wild-type glucocerebrosidase improves pathogenic phenotypes in dopaminergic neuronal models of Parkinson's disease. *Sci Transl Med*. 2019;11(514):eaau6870. doi:10.1126/scitranslmed.aau6870

56. Horowitz M, Pasmanik-Chor M, Ron I, Kolodny EH. The enigma of the E326K mutation in acid β-glucocerebrosidase. *Mol Genet Metab*. 2011;104(1-2):35-38. doi:10.1016/j.ymgme.2011.07.002

57. Fernandes HJR, Hartfield EM, Christian HC, et al. ER Stress and Autophagic Perturbations Lead to Elevated Extracellular α-Synuclein in GBA-N370S Parkinson's iPSC-Derived Dopamine Neurons. *Stem Cell Rep*. 2016;6(3):342-356. doi:10.1016/j.stemcr.2016.01.013

58. Kuo SH, Tasset I, Cheng MM, et al. Mutant glucocerebrosidase impairs α-synuclein degradation by blockade of chaperone-mediated autophagy. *Sci Adv*. 2022;8(6):eabm6393. doi:10.1126/sciadv.abm6393

59. Oslowski CM, Urano F. Measuring ER Stress and the Unfolded Protein Response Using Mammalian Tissue Culture System. In: *Methods in Enzymology*. Vol 490. Elsevier; 2011:71-92. doi:10.1016/B978-0-12-385114-7.00004-0

60. Bellucci A, Navarria L, Zaltieri M, et al. Induction of the unfolded protein response by α-synuclein in experimental models of Parkinson's disease: α-Synuclein accumulation induces the UPR. *J Neurochem*. 2011;116(4):588-605. doi:10.1111/j.1471-4159.2010.07143.x

61. Jo J, Yang L, Tran HD, et al. Lewy Body-like Inclusions in Human Midbrain Organoids Carrying Glucocerebrosidase and α-Synuclein Mutations. *Ann Neurol*. 2021;90(3):490-505. doi:10.1002/ana.26166

62. Kuusisto E, Parkkinen L, Alafuzoff I. Morphogenesis of Lewy Bodies: Dissimilar Incorporation of α-Synuclein, Ubiquitin, and p62. *J Neuropathol Exp Neurol*. 2003;62(12):1241-1253. doi:10.1093/jnen/62.12.1241

63. Scudamore O, Ciossek T. Increased Oxidative Stress Exacerbates α-Synuclein Aggregation In Vivo. *J Neuropathol Exp Neurol*. 2018;77(6):443-453. doi:10.1093/jnen/nly024

64. Moraitou M, Dermentzaki G, Dimitriou E, et al. α-Synuclein dimerization in erythrocytes of Gaucher disease patients: correlation with lipid abnormalities and oxidative stress. *Neurosci Lett*. 2016;613:1-5. doi:10.1016/j.neulet.2015.12.013

65. Mullin S, Smith L, Lee K, et al. Ambroxol for the Treatment of Patients With Parkinson Disease With and Without Glucocerebrosidase Gene Mutations: A Nonrandomized, Noncontrolled Trial. *JAMA Neurol*. 2020;77(4):427-434. doi:10.1001/jamaneurol.2019.4611

66. Giladi N, Alcalay RN, Cutter G, et al. Safety and efficacy of venglustat in GBA1-associated Parkinson's disease: an international, multicentre, double-blind, randomised, placebo-controlled, phase 2 trial. *Lancet Neurol*. 2023;22(8):661-671. doi:10.1016/S1474-4422(23)00205-3

67. Lunghi G, Carsana EV, Loberto N, et al. β-Glucocerebrosidase Deficiency Activates an Aberrant Lysosome-Plasma Membrane Axis Responsible for the Onset of Neurodegeneration. *Cells*. 2022;11(15):2343. doi:10.3390/cells11152343

68. Espay AJ, McFarthing K. Alpha-synuclein and the Parkinson's disease drug pipeline. *Parkinsonism Relat Disord*. 2023;111:105432. doi:10.1016/j.parkreldis.2023.105432

69. Zaltieri M, Grigoletto J, Longhena F, et al. α-synuclein and synapsin III cooperatively regulate synaptic function in dopamine neurons. *J Cell Sci*. 2015;128(13):2231-2243. doi:10.1242/jcs.157867

70. Faustini G, Longhena F, Masato A, et al. Synapsin III gene silencing redeems alpha-synuclein transgenic mice from Parkinson's disease-like phenotype. *Mol Ther*. 2022;30(4):1465-1483. doi:10.1016/j.ymthe.2022.01.021

71. Schidlitzki A, Stanojlovic M, Fournier C, et al. Double-Edged Effects of Venglustat on Behavior and Pathology in Mice Overexpressing α-Synuclein. *Mov Disord Off J Mov Disord Soc*. 2023;38(6):1044-1055. doi:10.1002/mds.29398

Figure legends

Figure 1 MOs display mature NM-containing DA neurons. (A) Schematic overview of the differentiation protocol for the generation of MOs. On day 0 (D0), iPSCs are seeded into ultra-low attachment plates to allow embryoid body formation (D0 – D6). Following neural induction, embryoid bodies are embedded in Cultrex (R&D) (D10) and cultured in static conditions for another 4 days. On D14, tissues are transferred to spinning bioreactors, where they are subdued to DA patterning factors. Trophic factors are added on D27 to aid DA maturation and long-term culturing. (B) Differentiation protocol efficiency measured as quantification of TH^+ cells over $NeuN^+$ nuclei in $CTR1^{wt}$ MOs at 65 DIV. Data are presented as mean ± s.e.m. (n = 4 organoids per condition were analysed by examining whole organoid volume). (C) Representative immunofluorescence images of $CTR1^{wt}$ MOs at 100 DIV showing TH and NeuN expression at different magnifications. Scale bars, 50 µm (*right*), 100 µm (*centre*), and 500 µm (*left*). (D-F) Representative immunofluorescence images of neuronal and DA markers (MAP2, TH, GIRK2) expression in $CTR1^{wt}$ MOs at 65 DIV. Arrowheads in (F) indicate cell bodies of TH^+/$GIRK2^+$ DA neurons. In (D) and (E), boxed areas are expanded in the corresponding insets. Scale bars, 25 µm (F), 100 µm (D *right*, E *right*), 200 µm (D *left*), and 500 µm (E *left*). (G) Sphingolipid composition of MOs (pool of CTR^{wt}, PD^{L444P}, and GD/PD^{L444P} MOs) at early (6 DIV) and mature (65 or 100 DIV) time points. Fully differentiated MOs have a higher content of gangliosides and

sphingomyelin enriched in human adult brain. Data are presented as mean ± s.e.m. (n = 12 organoids for each time point; ****P < 0.0001, two-tailed unpaired Student's t-test). (H) High magnification images of hematoxylin and eosin-stained sections of CTR1^{wt} MOs at 100 DIV demonstrates NM in neurons at single-cell resolution (arrowheads). Scale bars, 25 µm. (I) Hematoxylin and eosin staining (*left*) and Schmorl's ferricyanide reduction method (*right*) in serial sections of CTR2^{wt} (*upper*) and PD^{L444P} (*lower*) MOs at 120 DIV highlight the presence of NM pigmentation. Scale bars, 100 µm (*lower*) and 500 µm (*upper*). (J) Naturally pigmented neuromelanin granules (arrowheads) in TH^{+} neurons (red) in CTR2^{wt} MOs at 120 DIV. Scale bar, 10 µm. (K) TEM image of GD/PD^{L444P} MO at 80 DIV showing a membrane-bound (arrowheads) pigmented organelle containing NM granules (dark-coloured pigment) and vacuolar lipid body (asterisk) . Scale bar, 1 µm.

Abbreviations: ASAC, ascorbic acid. BDNF, brain-derived neurotrophic factor. bFGF, basic fibroblast growth factor. cAMP, cyclic adenosine monophosphate. DIV, days *in vitro*. EB, embryoid body. FGF8b, fibroblast growth factor 8b. GDNF, glial cell line-derived neurotrophic factor. GIRK2, G-protein-regulated inward-rectifier potassium channel 2. hES, human embryonic stem cells. KSR, knock-out serum replacement. MAP2, microtubule-associated protein 2. MO, midbrain organoid. NeuN, Neuronal Nuclei. NM, neuromelanin. PURM, purmorphamine. SAG, smoothened agonist. SM, sphingomyelin. TEM, transmission electron microscopy. TGFb3, transforming growth factor beta-3. TH, tyrosine hydroxylase.

Figure 2 *GBA1* L444P mutation results in reduced enzyme activity, ER retention of mutant GCase, and increased levels of GlcCer. (A) GCase enzymatic activity in CTR^{wt} MOs at 65 DIV with and without treatment with 500 µM CBE for 14 days. Data are presented as mean ± s.e.m. (n = 9 organoids; ****P < 0.0001, two-tailed unpaired Student's t-test). (B) GCase enzymatic activity in CTR^{wt}, PD^{L444P}, and GD/PD^{L444P} MOs at 6, 65, 100, and 150 DIV. Data are presented as mean ± s.e.m. (n = 3 biological replicates per line for each time point; ****P < 0.0001, ***P < 0.001, two-way ANOVA with Dunnett's post hoc test). (C) GCase enzymatic activity in SNc_CTR^{wt} and SNc_PD^{L444P} brain extracts. Data are presented as mean ± s.e.m. (n = 12 samples; **P < 0.01, two-tailed unpaired Student's t-test). (D and E) Representative Western blots and relative densitometries showing GCase levels in CTR^{wt}, PD^{L444P}, and GD/PD^{L444P} MOs at 50, 100, and 150

DIV. Data are presented as mean ± s.e.m. (n = 33 organoids; ****P < 0.0001, ***P < 0.001, **P < 0.01, *P < 0.05, two-way ANOVA with Dunnett's post hoc test). (F) Densitometry of GCase/GAPDH amount in patients' brain extracts. Data are presented as mean ± s.e.m. (n = 9 samples; **P < 0.01, two-tailed unpaired Student's t-test). (G) Representative images of CTR^{wt}, PD^{L444P}, and GD/PD^{L444P} MOs at 100 DIV immunolabelled for GCase, Grp78, and ERp72. Indicated regions are expanded in the insets below. Scale bars, 5 µm (*lower*) and 10 µm (*upper*). (H) Quantification of Grp78, Grp78/GCase co-localization, and ERp72/GCase co-localization from immunofluorescent images shown in (G). Data are presented as mean ± s.e.m. (n = 3 biological replicates per line; ***P < 0.001, **P < 0.01, *P < 0.05, one-way ANOVA with Tukey's post hoc test). (I) Densitometry of p-eIF2α/GAPDH amount in CTR^{wt}, PD^{L444P}, and GD/PD^{L444P} MOs at 50 and 80 DIV. Data are presented as mean ± s.e.m. (n = 21 organoids; **P < 0.01, *P < 0.05, two-way ANOVA with Dunnett's post hoc test). (J and K) GlcCer levels in CTR^{wt} MOs at 65 DIV following treatment with CBE (J) and in CTR^{wt}, PD^{L444P}, and GD/PD^{L444P} MOs at 6, 65, 100, and 150 DIV (K) evaluated by the metabolic labelling at the steady state using radioactive sphingosine. Data are presented as mean ± s.e.m. [in (J): n = 9 organoids; ****P < 0.0001, two-tailed unpaired Student's t-test; in (K): n = 3 biological replicates per line for each time point; ****P < 0.0001, two-way ANOVA with Dunnett's post hoc test]. Abbreviations: A.U., arbitrary units. CBE, conduritol B epoxide. CTR^{wt}, control subject. DIV, days *in vitro*. ERp72, endoplasmic reticulum protein 72. GCase, glucocerebrosidase. GD/PD^{L444P}, Gaucher's disease/Parkinson's disease patient carrying homozygous L444P *GBA1* mutation. GlcCer, glucosylceramide. Grp78, glucose-regulated protein 78. LAMP1, lysosomal-associated membrane protein 1. PD^{L444P}, Parkinson's disease patient carrying heterozygous L444P *GBA1* mutation. p-eIF2α, phosphorylated Eukaryotic translation initiation factor 2 subunit 1. SNc_CTR^{wt}, substantia nigra from *post-mortem* brain of a healthy donor. SNc_PD^{L444P}, substantia nigra from *post-mortem* brain of Parkinson's disease patient carrying heterozygous L444P *GBA1* mutation. UNTR, untreated.

Figure 3 *GBA1*-PD MOs reproduce DA neurodegeneration and Lewy-like pathology. (A and B) Immunofluorescence labelling of TDE-clarified CTR^{wt}, PD^{L444P}, and GD/PD^{L444P} MOs at 100 DIV and relative 3D confocal microscopy analysis of TH^+ and $NeuN^+$ cells showing DA neuron loss in *GBA1* mutant MOs. Images in (A) show orthogonal z-stack projections. Data are presented as mean ± s.e.m. (n = 14 organoids, each value in the graph corresponds to analysis conducted on

individual whole organoids; ***$P < 0.001$, **$P < 0.01$, one-way ANOVA with Dunnett's post hoc test). Scale bars, 100 µm (*lower*) and 500 µm (*upper*). (C) Analysis of the progressive accumulation of α-syn in TH^+ neurons in *GBA1* mutant MOs from immunostaining shown in Supplementary Fig. 7A. Data are presented as mean ± s.e.m. ($n = 2$ organoids of each line were analysed by examining an average of 5 fields per condition; ****$P < 0.0001$, ***$P < 0.001$, **$P < 0.01$, two-way ANOVA with Tukey's post hoc test). (D and E) Representative Western blots and relative densitometry of detergent-resistant insoluble α-syn fractions in CTR^{wt}, PD^{L444P}, and GD/PD^{L444P} MOs at 60 and 80 DIV. Asterisk indicates a non-specific 55 kDa band. Data are presented as mean ± s.e.m. ($n = 3$ biological replicates per line at 60 DIV, $n = 5$ biological replicates per line at 80 DIV; ****$P < 0.0001$, *$P < 0.05$, one-way ANOVA with Dunnett's post hoc test). (F) Representative IHC images of PK-resistant insoluble α-syn immunoreactivity (BioLegend 847902) in CTR^{wt}, PD^{L444P}, and GD/PD^{L444P} MOs at 80 DIV. Scale bars, 25 µm. (G) DAB immunoreactivity of α-syn (BioLegend 847902) in eosin-stained CTR^{wt}, PD^{L444P}, and GD/PD^{L444P} MOs at 80 DIV and in SNc_PD^{L444P} following treatment with PK. Arrowheads indicate PK-resistant inclusions of insoluble α-syn. Scale bars, 25 µm. (H and I) High magnification images of PK-resistant α-syn (BioLegend 847902) organization in MOs from subjects carrying L444P *GBA1* mutations at 100 DIV and in SNc_PD^{L444P}: heterogeneous morphology of α-syn inclusions may be indicative of various stages of maturation of LB-like aggregates (H) and LN-like processes (I) reminiscent of Lewy pathology seen in human brains (arrowheads). Scale bars, 5 µm. (J and K) Immunostaining of pS129 α-syn inclusions in TH^+ neurons (J) and quantification of pS129 $\alpha\text{-syn}^+$ area (K) in CTR^{wt}, PD^{L444P}, and GD/PD^{L444P} MOs at 100 DIV. Images in (J) show orthogonal z-stack projections. Data are presented as mean ± s.e.m. ($n = 5$ biological replicates per line, with each point representing the mean of 3 z-stack images for each organoid; **$P < 0.01$, *$P < 0.05$, one-way ANOVA with Dunnett's post hoc test). Scale bars, 5 µm (*lower*) and 10 µm (*upper*). (L) Representative TEM images of PD^{L444P} (*left*) and GD/PD^{L444P} (*right*) MOs at 80 DIV showing large autophagosome/autolysosome-like bodies (highlighted in orange) with inclusions of aggregated intracellular material in the perinuclear region. Boxed areas are expanded in the corresponding insets. Cellular organelles are indicated by asterisks and in the corresponding legend. Scale bars, 500 nm (*lower right*), 1 µm (*lower left*), and 2 µm (*upper*). (M) Representative TEM images of a Lewy-like inclusion (highlighted in orange) in PD^{L444P} MO at 80 DIV. Disrupted cytoskeleton and filaments (orange arrows), tubulovesicular structures (blue arrows), lipid droplets

(aqua asterisk), abundant membrane fragments from mitochondria (pink asterisks) and lysosomes (green asterisks) are visible. Boxed areas are expanded in the insets. Scale bars, 500 nm (*lower left*), 1 µm (*right*), and 5 µm (*upper left*). Abbreviations: α-syn, α-synuclein. A.U., arbitrary units. CTR^{wt}, control subject. DIV, days *in vitro*. GD/PD^{L444P}, Gaucher's disease/Parkinson's disease patient carrying homozygous L444P *GBA1* mutation. LB, Lewy body. LN, Lewy neurite. MO, midbrain organoid. pS129 α-syn, phospho-α-synuclein (Ser129). PD^{L444P}, Parkinson's disease patient carrying heterozygous L444P *GBA1* mutation. PK, proteinase K. SNc_PD^{L444P}, substantia nigra from *post-mortem* brain of Parkinson's disease patient carrying heterozygous L444P *GBA1* mutation. TH, tyrosine hydroxylase.

Figure 4 Insoluble α-syn from *GBA1* MOs induces aggregation of endogenous α-syn. (A) Representative immunofluorescence images of $α\text{-syn}^+/\text{Thio-S}^+$ aggregates in TH^+ neurons in PD^{L444P} and GD/PD^{L444P} at 100 DIV and in CBE-treated CTR^{wt} MOs. Arrowheads indicate inclusions of fibrillary α-syn with double staining for α-syn and Thio-S. Scale bars, 25 µm. (B) Analysis of the percentage of α-syn in TH^+ neurons in CTR^{wt} MOs at 100 DIV following CBE treatment shown in (A). Data are presented as mean ± s.e.m. ($n = 3$ organoids per condition; $^{****}P < 0.0001$, two-tailed unpaired Student's t-test). (C) Analysis of the overlay area of Thio-S/α-syn in CBE-treated CTR^{wt} MOs at 100 DIV shown in (A). Data are presented as mean ± s.e.m. ($n = 3$ organoids per condition; $^{****}P < 0.0001$, two-tailed unpaired Student's t-test). (D) Analysis of the overlay area of Thio-S/α-syn in CTR^{wt}, PD^{L444P}, and GD/PD^{L444P} MOs at 100 DIV shown in (A). Data are presented as mean ± s.e.m. ($n = 14$ organoids; $^{****}P < 0.0001$, $^{***}P < 0.001$, one-way ANOVA with Tukey's post hoc test). (E) Aggregation kinetics of recombinant α-syn induced by CTR^{wt}, PD^{L444P}, and GD/PD^{L444P} MOs at 100 DIV and brain homogenates (BH) of the PD^{L444P} patient (SNc_PD^{L444P}) and one control subject (SNc_CTR^{wt}). (F) Representative IHC images of α-syn and Thio-S-labelled aggregates in $β3TUB^+$ neurons in $CTR3^{wt}$ MOs at 100 DIV previously injected with α-syn extracted from PD^{L444P} MOs or $CTR1^{wt}$ MOs at 100 DIV. Arrowheads indicate inclusions of fibrillary α-syn with double staining for α-syn and Thio-S. Boxed areas are expanded in the insets on the right. Scale bars, 25 µm. (G) Analysis of the overlay area of Thio-S/α-syn in $CTR3^{wt}$ MOs following injection of α-syn from data shown in (F). Data are presented as mean ± s.e.m. ($n = 4$ organoids per condition; $^{**}P < 0.01$, two-tailed unpaired Student's t-test).

Abbreviations: α-syn, α-synuclein. A.U., arbitrary units. β3TUB, β-3 tubulin. BH, brain homogenate. CBE, conduritol B epoxide. CTR^{wt}, control subject. DIV, days *in vitro*. GD/PD^{L444P}, Gaucher's disease/Parkinson's disease patient carrying homozygous L444P *GBA1* mutation. MO, midbrain organoid. PD^{L444P}, Parkinson's disease patient carrying heterozygous L444P *GBA1* mutation. SAA, seed amplification assay. Thio-S, thioflavin-S. UNTR: untreated.

Figure 5 Rescue of GCase pathway and α-syn pathology with ambroxol and GZ667161. (A-D) Representative Western blots and relative densitometry of GCase protein amount in CTR^{wt}, PD^{L444P}, and GD/PD^{L444P} MOs at 100 DIV with and without treatment with ambroxol (100 μM for 10 days) (A and B) or GZ667161 (100 nM for 14 days) (C and D) calculated as percentage changes with respect to untreated. Data are presented as mean ± s.e.m. (n = 4-16 organoids per condition; $^{****}P < 0.0001$, $^{**}P < 0.01$, $^{*}P < 0.05$, two-tailed unpaired Student's t-test). (E and F) GlcCer levels of CTR^{wt}, PD^{L444P}, and GD/PD^{L444P} MOs at 100 DIV with and without treatment with ambroxol or GZ667161 evaluated by the metabolic labelling at the steady state using [1-^{3}H]sphingosine. Data are presented as mean ± s.e.m. [n = 4 biological replicates per line per condition in (E); n = 3-5 biological replicates per line per condition in (F); $^{****}P < 0.0001$, $^{***}P < 0.001$, two-way ANOVA with Tukey's post hoc test]. (G) Co-localization percentage of LAMP1 and GCase in PD^{L444P} and GD/PD^{L4444P} MOs at 100 DIV from immunofluorescence images shown in Supplementary Fig. 10C. Data are presented as mean ± s.e.m. (n = 3 biological replicates per line; $^{***}P < 0.001$, $^{**}P < 0.01$, $^{*}P < 0.05$, one-way ANOVA with Dunnett's post hoc test). (H and I) Representative immunofluorescence images of PK-resistant insoluble α-syn immunoreactivity (BioLegend 824301) in CTR^{wt}, PD^{L444P}, and GD/PD^{L444P} MOs at 100 DIV with and without treatment with ambroxol or GZ667161 (H) and quantification of α-syn aggregates number per field and relative percentage changes in α-syn area with respect to untreated (I). Data are presented as mean ± s.e.m. (n = 3 organoids for each line were analysed by examining an average of 5 fields per condition from different sections; $^{****}P < 0.0001$, $^{***}P < 0.001$, $^{**}P < 0.01$, $^{*}P < 0.05$, one-way ANOVA with Dunnett's post hoc test). Scale bar, 25 μm. Abbreviations: α-syn, α-synuclein. AMBR, ambroxol. Cer, ceramide. CTR^{wt}, control subject. DIV, days *in vitro*. GCase, glucocerebrosidase. GD/PD^{L444P}, Gaucher's disease/Parkinson's disease patient carrying homozygous L444P *GBA1* mutation. GlcCer, glucosylceramide. LAMP1, lysosomal-associated

membrane protein 1. PD^{L444P}, Parkinson's disease patient carrying heterozygous L444P *GBA1* mutation. PK, proteinase K. UNTR, untreated.

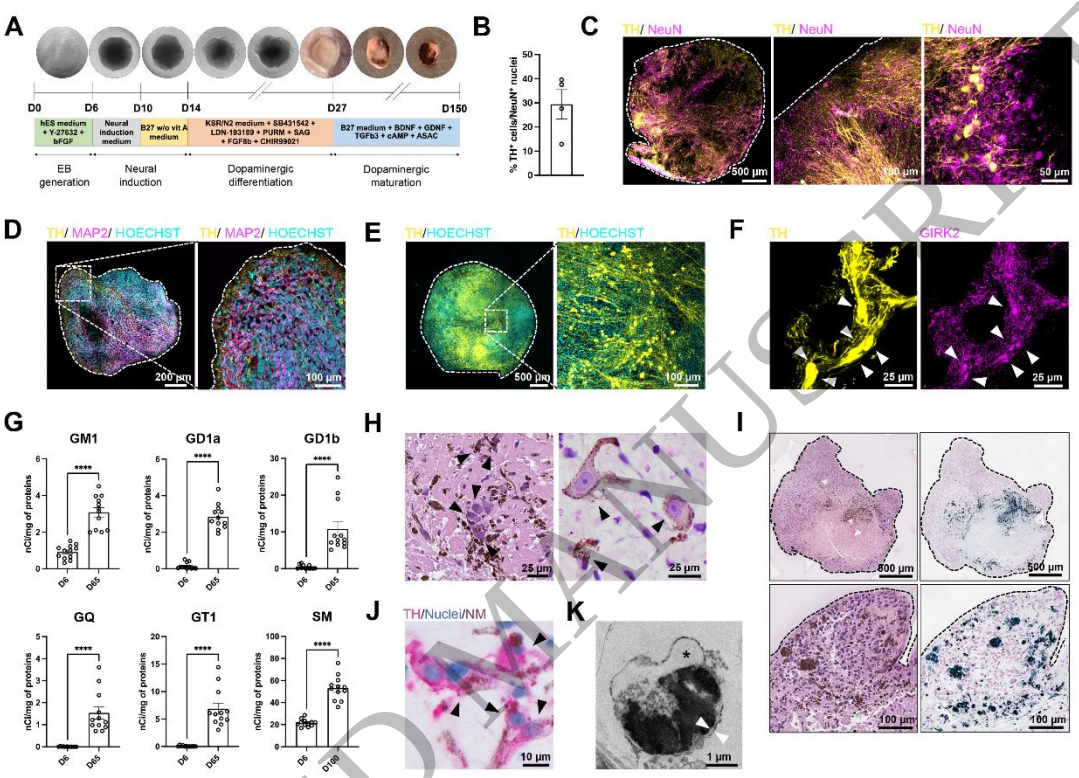

Figure 1
146x106 mm (x DPI)

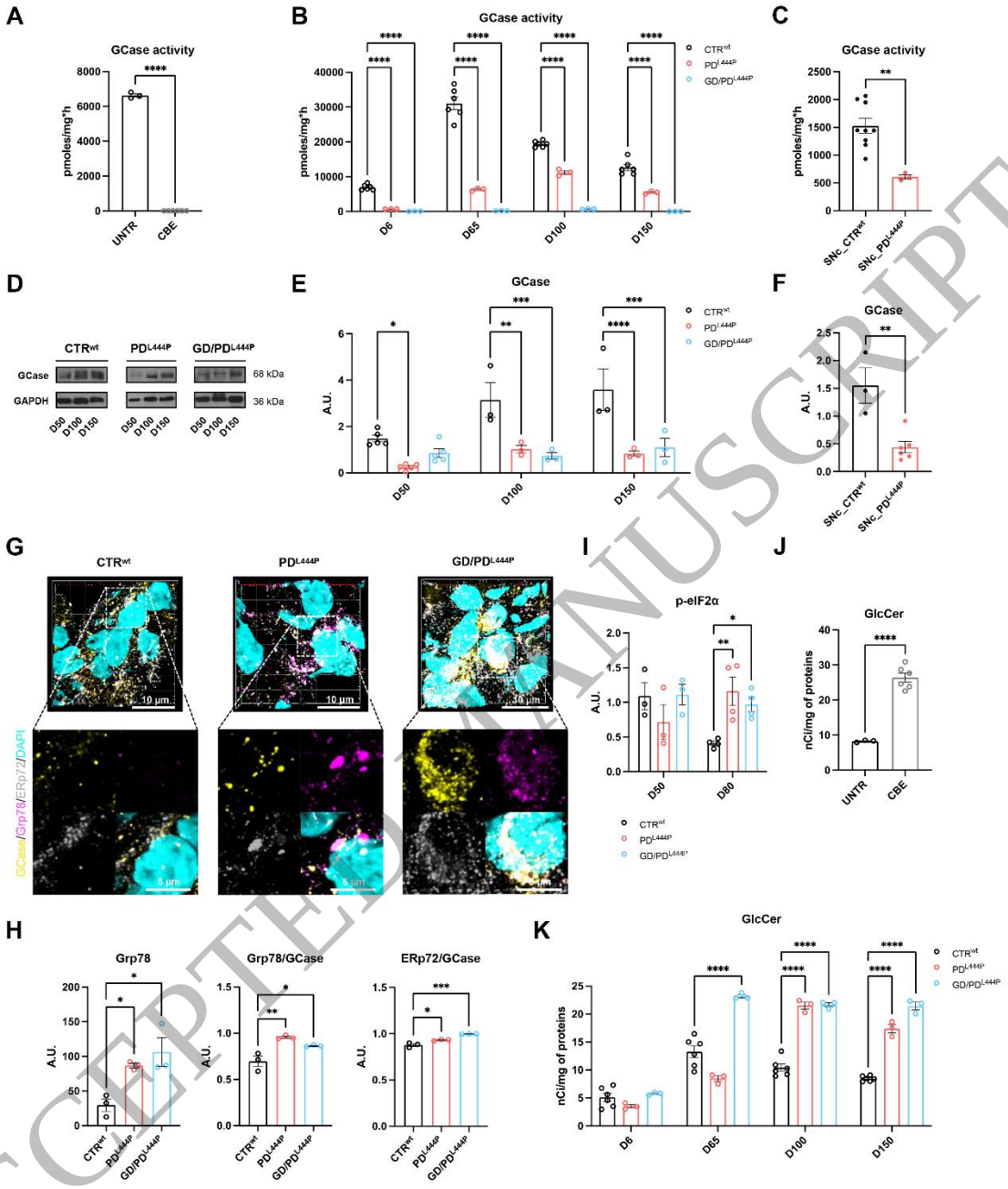

Figure 2
151x176 mm (x DPI)

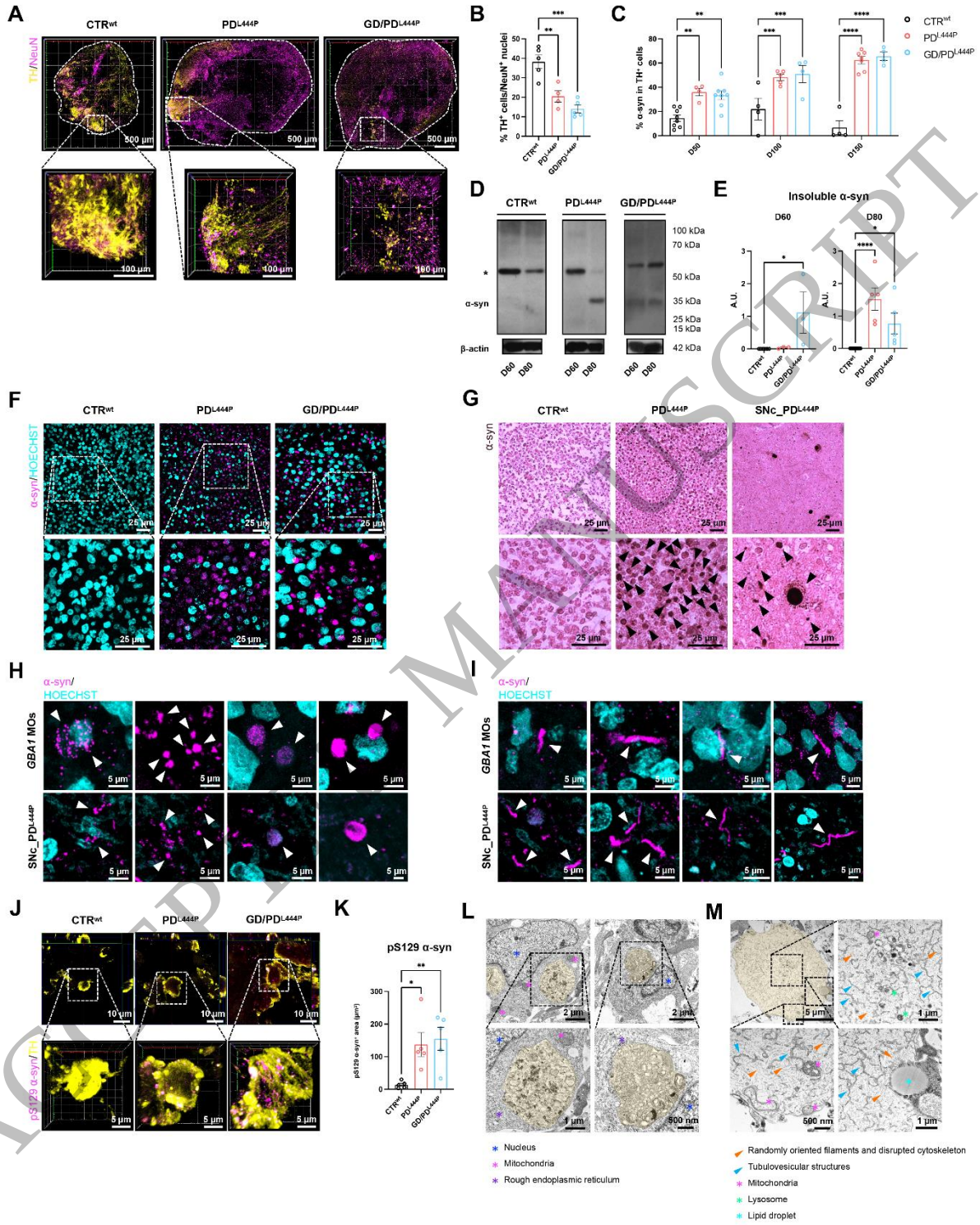

Figure 3
164x205 mm (x DPI)

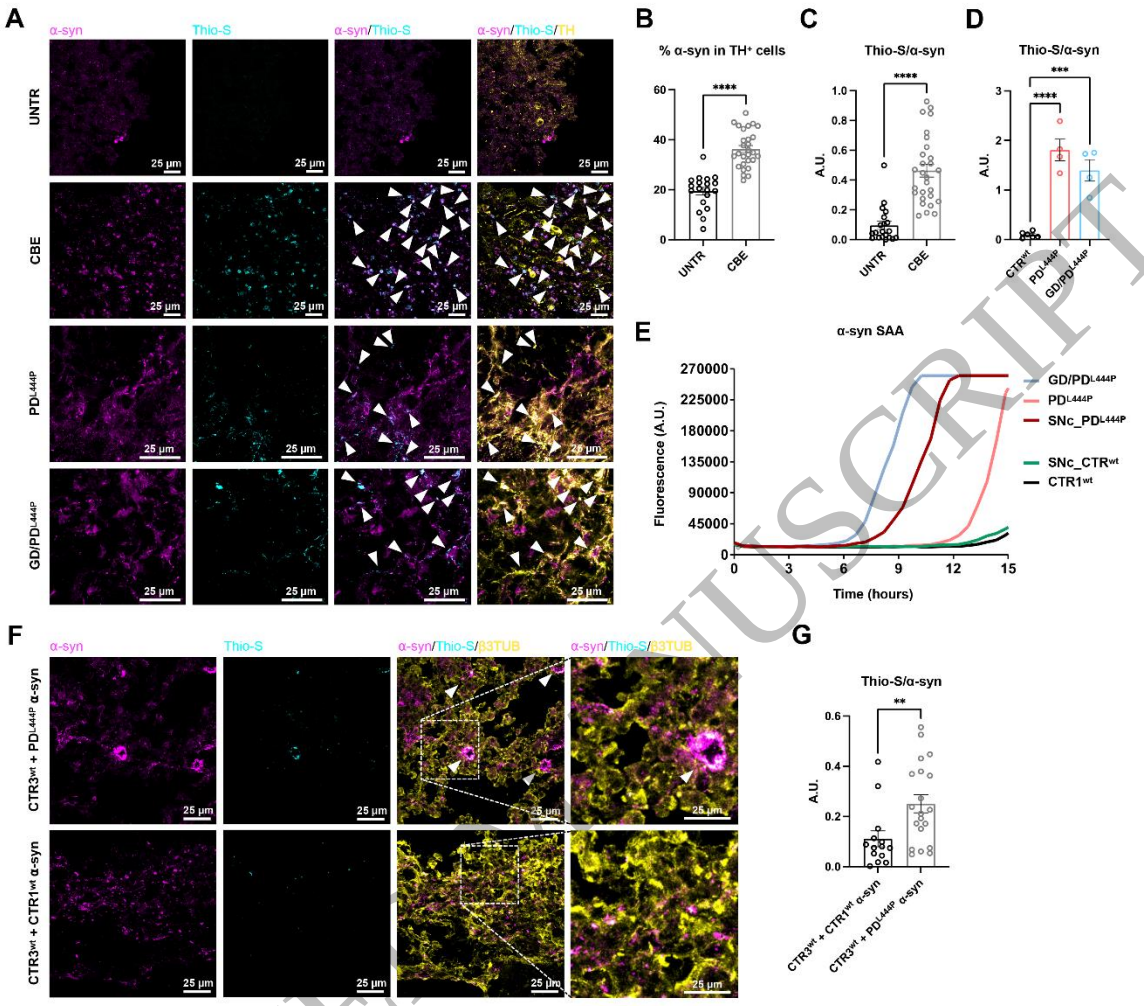

Figure 4
153x136 mm (x DPI)

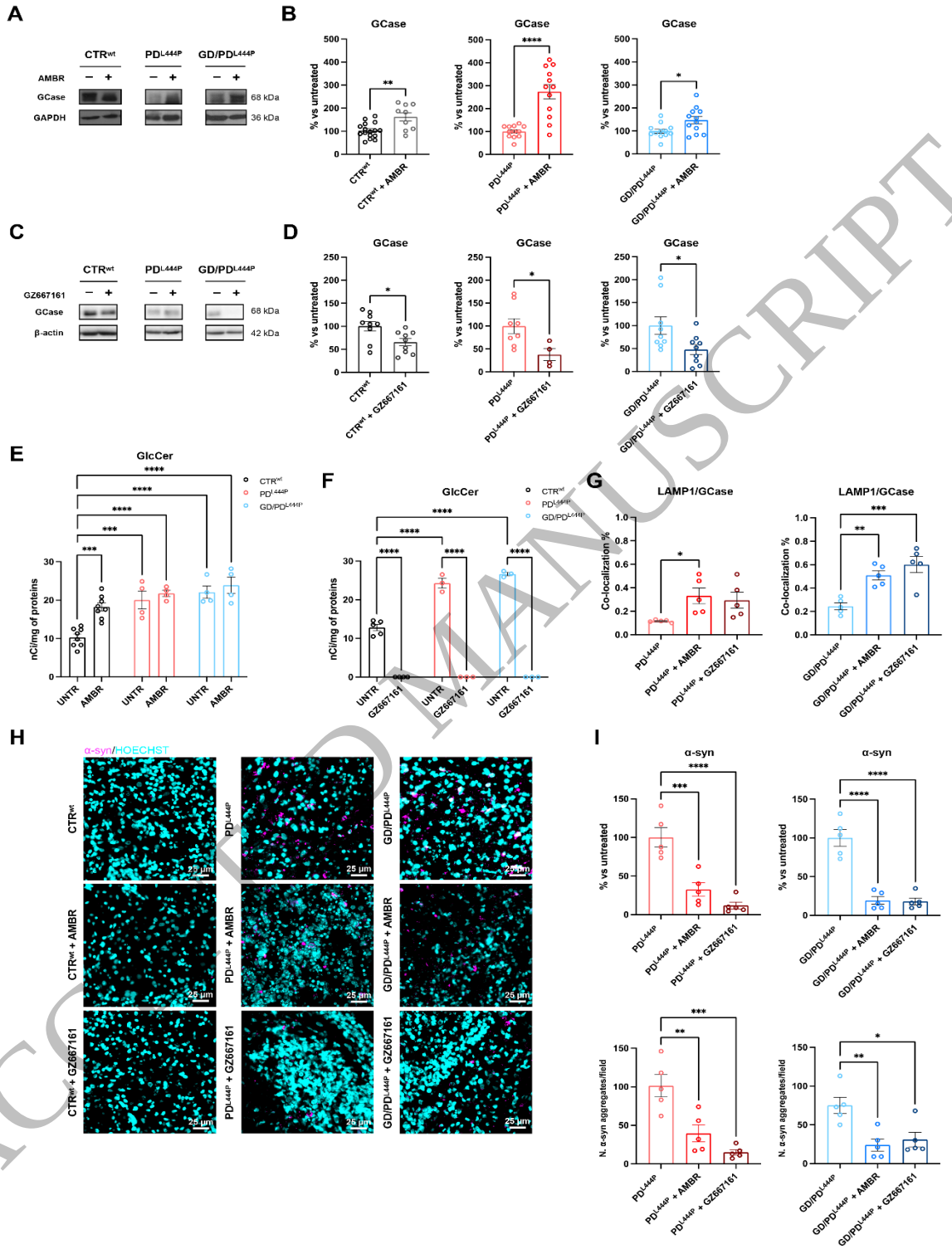

Figure 5
155x218 mm (x DPI)